

TECHNICAL UNIVERSITY OF CRETE  
ELECTRONIC AND COMPUTER ENGINEERING DEPARTMENT  
TELECOMMUNICATIONS DIVISION



# Bistatic Scatter Radio for Increased-range Environmental Sensing

by

John Kimionis

A THESIS SUBMITTED IN PARTIAL FULFILLMENT OF  
THE REQUIREMENTS FOR THE MASTER OF SCIENCE OF  
ELECTRONIC AND COMPUTER ENGINEERING

August 2013

## THESIS COMMITTEE

Assistant Professor Aggelos Bletsas, *Thesis Supervisor*  
Associate Professor George N. Karystinos  
Professor Athanasios P. Liavas

# Abstract

For environmental sensing applications that require dense deployments, scatter radio is a promising communication scheme. Since modulation is achieved by means of reflection, very low-cost and low-power RF front-ends are required. However, its use in sensor networks has been limited, since commercial scatter radio applications, like RFID, are limited to ranges of a few meters. To overcome this limitation, bistatic scatter radio architectures are exploited, that boost the operating range up to 130 meters with only 20 milliwatts of carrier power. The carrier emitter is detached from the reader to form a cell wherein sensors-modulators may reside and communicate efficiently. As conventional radio receivers are not directly applicable, the complete signal model is derived (i.e. not assumed) for the bistatic scatter radio link, by exploiting both communication theory and microwave theory. A simple on-off-keying (OOK) modulation scheme appropriate for the bandwidth-limited regime is presented with non-linear receivers that overcome the carrier frequency offset between the carrier emitter and the reader. Also, noncoherent frequency-shift-keying (FSK) is described for the power-limited regime, that accounts for sensor multiple access through frequency division multiplexing. This scheme is shown to achieve a robust bit-error-rate (BER) performance at the receiver, immune to channel conditions changes and is therefore convenient for the low-bitrate nature of environmental sensing. This work discusses the impact of important microwave parameters such as the antenna structural mode on the receiver performance. It is shown that tags and their corresponding receivers should be jointly designed to maximize BER performance. Outdoor experimental measurements with a custom setup prove the long-range capability of bistatic scatter radio architectures.

Thesis Supervisor: Assistant Professor Aggelos Bletsas

# Acknowledgements

As my MS studies are now coming to an end, I must say that the last two years have been really important to me. Lots of ups and downs, a lot of work, a lot of fun; everything contributed to form a great combination. My supervisor, Prof. Aggelos Bletsas, was the mentor who pointed me out that you have to work hard to achieve high quality results. He opened my way in the world of research, which I now follow with no fear. I wholeheartedly thank him for this. My family supported me in every way while studying and kept encouraging me every single moment. With my friends we shared all funny moments; they were the excuse to take little, enjoyable breaks from work, and-trust me-that really helped. My girlfriend was maybe the greatest supporter these years: encouragement, tolerance, motivation. She has always been there for me and ensured that I stay on balance. I am now ready to continue my studies and work, with beautiful moments on my mind, and much greater experience. No obstacles, only challenges!

*To my family, friends, and Electra..*

# Table of Contents

<b>Table of Contents</b> . . . . .	4
<b>List of Figures</b> . . . . .	6
<b>List of Tables</b> . . . . .	8
<b>1 Scatter Radio for Environmental Sensing.</b> . . . . .	9
1.1 Large-scale WSNs . . . . .	9
1.2 Scatter Radio . . . . .	10
1.3 Topology - Why bistatic . . . . .	11
<b>2 Scatter Radio Modules</b> . . . . .	14
2.1 Setup . . . . .	14
2.2 RF Tag Design . . . . .	15
2.3 Carrier Emitter & Reader . . . . .	17
<b>3 Bistatic Scatter Radio Links</b> . . . . .	19
3.1 Signal model . . . . .	19
3.2 Modulation Schemes & Receivers . . . . .	23
3.2.1 OOK . . . . .	24
3.2.2 FSK . . . . .	30
3.2.3 Carrier Recovery . . . . .	35
<b>4 Performance</b> . . . . .	36
4.1 BER Performance . . . . .	36
4.1.1 OOK . . . . .	36
4.1.2 FSK . . . . .	41
4.1.3 Modulation Comparison . . . . .	43

---

4.2	Achieved Bistatic Ranges . . . . .	44
4.2.1	Tag close to carrier emitter . . . . .	45
4.2.2	Tag behind carrier emitter . . . . .	47
4.2.3	Tag close to reader . . . . .	48
4.2.4	Triangle topology . . . . .	48
4.2.5	Results . . . . .	49
4.3	Antenna measurements . . . . .	50
<b>5</b>	<b>Conclusions</b> . . . . .	<b>53</b>
5.1	Conclusion . . . . .	53
5.2	Future Work . . . . .	54
<b>6</b>	<b>Appendix</b> . . . . .	<b>56</b>
6.1	Proofs . . . . .	56
6.1.1	Noise PSD . . . . .	56
6.1.2	Orthogonality of FSK base functions . . . . .	57
6.1.3	Noise Variance for FSK receiver BER . . . . .	58
6.2	RF Tag Schematics & Bill of Materials . . . . .	59
	<b>Bibliography</b> . . . . .	<b>62</b>

# List of Figures

1.1	Bistatic scatter radio setup overview. . . . .	11
1.2	Scatter radio field with sensors/RF tags. Multiple carrier emitters are placed in the field to illuminate tags, along with a centralized receiver (reader). . . . .	12
2.1	Bistatic scatter radio setup. . . . .	14
2.2	Semi-passive tag prototype with its coin battery. . . . .	15
2.3	Scatter radio modulation with RF transistor. . . . .	16
2.4	Carrier emitter evaluation board. . . . .	17
2.5	SDR Reader consisting of commodity SDR hardware and a PC performing all signal processing. . . . .	18
3.1	Bistatic channel model: carrier emitter is dislocated from the receiving reader and RF tag acts as the signal modulator. . . . .	19
3.2	Left: Baseband OOK backscattered signal and its corresponding spectrum. Right: Baseband FSK backscattered signal and its corresponding spectrum. . . . .	24
3.3	Signal processing chain for OOK data. . . . .	28
3.4	Complex baseband spectrum for scatter radio FSK (left) and ‘classic’ FSK (right). Two subcarriers per frequency exist in scatter radio FSK, in contrast with classic FSK. . . . .	31
3.5	FSK signal processing chain. After CFO compensation and DC-blocking, the complex baseband signal is correlated against $\pm F_0, \pm F_1$ for $L$ samples, which correspond to one bit duration $T$ . Then, the correlator outputs are sampled and detection is performed on the samples. . . . .	33

---

4.1	Bit error rate for OOK ML and the approx-ML detector, with $L = 10$ . . . . .	39
4.2	Bit error rate of the OOK heuristic detector, with $L = 10$ . . .	40
4.3	Comparison of OOK approx-ML and heuristic detectors. . . .	40
4.4	Bit error probability as a function of SNR for scatter radio FSK, for no CFO and compensated CFO scenarios with $a_{\text{CR}} = 0$ .	43
4.5	Modulation comparison for the bistatic scatter radio link. FSK and OOK compared in terms of BER as a function of the emitter transmit power and the emitter-to-reader channel factor $a_{\text{CR}}$ . . . . .	45
4.6	Left: RF tag prototype. Right: Carrier emitter. . . . .	46
4.7	Experimental bistatic setup. . . . .	47
4.8	Experimental setup outdoor deployment. . . . .	47
4.9	Setup 1. . . . .	48
4.10	Setup 2. . . . .	48
4.11	Setup 3. . . . .	48
4.12	Setup 4. . . . .	49
4.13	RF tag prototype with commercial monopole antenna. . . . .	51
4.14	RF tag prototype with custom bow-tie antenna. . . . .	51
6.1	RF tag schematic. . . . .	59
6.2	RF tag PCB layout. . . . .	60

# List of Tables

4.1	Achieved ranges for Setup 1. . . . .	46
4.2	Achieved ranges for Setup 2. . . . .	48
4.3	Achieved ranges for Setup 3. . . . .	49
4.4	Achieved ranges for Setup 4. . . . .	49
6.1	Bill of Materials for semipassive RF tag. . . . .	61

# Chapter 1

## Scatter Radio for Environmental Sensing.

### 1.1 Large-scale WSNs

In this modern era, the necessity for closing the gap between technology and the physical environment is constantly growing. As people exploited natural resources to build high technology, it is now the time to exploit this technology to give back to the environment. Several examples that obligate this thoughtfulness exist: water-saving, wildlife and forest conservation, etc. An interesting practice which is embraced by farmers lately is precision agriculture that results in water-saving and production growth. With the advance of sensor technology and wireless networking, ubiquitous sensors can reinforce precision agriculture techniques by speeding up the information collection about environmental conditions on cultivations and greenhouses [1–3]. Wireless sensor networks (WSNs) can be utilized to monitor environmental parameters such as air and soil humidity, temperature, chlorophyll levels, soil PH, and others by attaching appropriate sensors to a WSN node. Such applications may require ultra dense networks of hundreds or thousands of nodes, to report information of *each* plant's microclimate.

The existing commercial WSN technologies utilize radios for wireless connectivity such as ZigBee, Bluetooth and the like [4]. These Marconi-type radios are usually the overhead for both the monetary cost and the energy consumption of a WSN node, because of the complex active radio frequency (RF) components they incorporate, such as amplifiers, mixers, and high quality filters. The high cost per node along with the high energy demands are prohibiting factors for the scalability of a WSN to dense network levels. Thus,

---

conventional WSN technologies cannot serve very large scale environmental sensing under a relatively low budget or very limited energy resources.

## 1.2 Scatter Radio

Instead of actively radiating power to transmit information, a node may *reflect* induced RF signals to modulate data. The scatter radio principle is based on centrally generating a carrier wave that illuminates many nodes (RF tags). A tag's antenna is connected to an impedance switch that changes the antenna load according to the transmitted data. Different loads have the effect of changing the induced signal's amplitude or phase or both. That way, the signal is modulated and reflected (scattered back) from the same antenna [5]. The scattered (or backscattered) signals are captured by a receiver (reader) which demodulates and decodes information from each tag.

Although scatter radio is not a new idea (first principles presented in [6]), it has only recently been utilized widely and for very specific purposes. The most prominent commercial use of scatter radio is in radio frequency identification (RFID) applications, for identifying people or products in supply chains. Commercial standards have been developed for RFID, albeit focusing on identification/supply chain applications only [7]. However, this communication scheme can be valuable to other scenarios as well, like wireless sensor networks (WSNs). Because communication can be achieved with a single radio frequency (RF) transistor front-end, scatter radio can minimize both energy requirements and monetary cost of a sensor node. This allows then for large scale sensor deployments, in contrast with existing WSN systems. Recent work has shown proof of concept systems that can be used in dense scatter radio networks. All those systems are built with low-cost and low-energy principles in mind [8–11].

An overview of the scatter radio architecture used throughout this work is given in Fig. 1.1: A carrier emitter transmits a single tone continuous wave (CW) to illuminate the RF tag, which modulates and backscatters information. A reader picks up the backscattered signals and decodes them to bits. The system follows a *bistatic* architecture; this means that the carrier wave

is generated from a terminal other than where the backscattered signals are received [12]. This is in contrast with monostatic setups that are commonly used in RFID systems and incorporate the carrier emitter and the receiver in a single reader box [5].

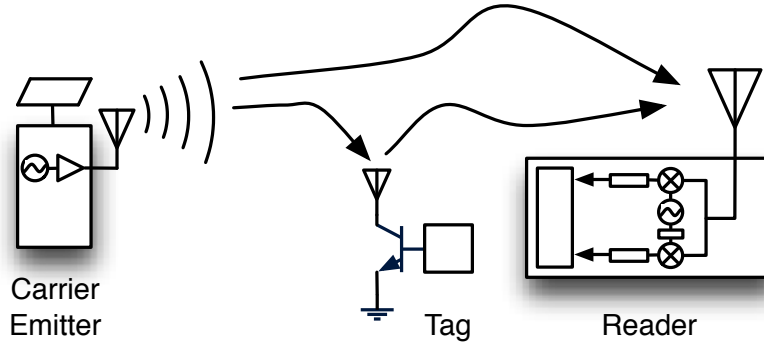


Figure 1.1: Bistatic scatter radio setup overview.

### 1.3 Topology - Why bistatic

Extended field coverage with sensor nodes is needed for agricultural networks. This means that the range for the point-to-point links between the sensor *tags* and a *reader* has to be maximized. However, for typical RFID applications, the achieved ranges are inherently limited due to the following reasons:

1) *Passive communication*: *Passive* tags are used, which require energy harvesting to power their electronics. Commonly, these tags rectify a continuous wave (CW) signal, transmitted by the reader. Thus, the achieved range is limited by the so-called “power-up link” [5].

2) *High bitrate*: Commercial RFID systems exploit high bitrates for tag-to-reader communication, on the order of hundreds of kbps. This means a small bit duration, resulting in reduced energy-per-bit and signal-to-noise ratio (SNR).

3) *Monostatic architecture*: The reader box consists of both the transmitter that emits the wave needed for backscatter communication and the receiver that decodes the tag-modulated signals. This means that typical

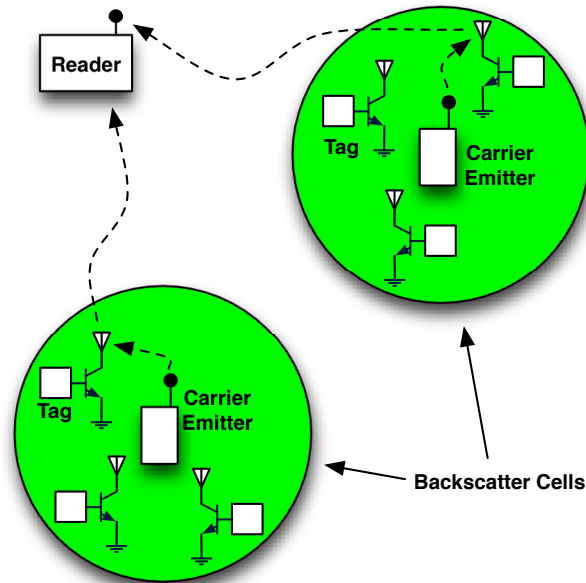


Figure 1.2: Scatter radio field with sensors/RF tags. Multiple carrier emitters are placed in the field to illuminate tags, along with a centralized receiver (reader).

RFID systems suffer from round-trip path loss; specifically SNR at the receiver drops with the fourth power of reader-to-tag distance [12], or the eighth power of the distance, for a two-ray propagation model [13, 14]. In monostatic setups, the tags that lay close to the reader are benefitted from the small distance, while tags that lay far are difficult to be “heard” from the reader. This causes a circular area around the reader, where coverage is limited.

Therefore, scatter radio has to be redesigned to accommodate WSN applications. To achieve long ranges and extended field coverage, prior art in [9] has directed two key points:

- 1) Semipassive tags (i.e. energy-assisted) have to be utilized. The tags may power their electronics by batteries, or low-cost renewable energy sources like low-voltage solar-cells [15].

- 2) Bitrate should be minimized, to maximize energy-per-bit at the receiver. Although high bitrates are appealing, they are not a necessity for environmental conditions monitoring, because parameters like humidity or

---

temperature change relatively slow. This allows for bigger duty cycles, with maximized bit durations and longer tag sleep periods to conserve energy.

In this work, a third point is proposed to achieve long range scatter radio communication for sensor networks. Particularly, *bistatic* architectures should be exploited. By dislocating the carrier emitter from the receiver, new, more flexible topologies can be set up. Carrier emitters may come in the form of an oscillator and a power amplifier only, and can thus be two orders of magnitude cheaper than the receiver/reader. The reader can be a low-cost software defined radio (SDR), which offers the flexibility of decoding multiple, arbitrary tag modulation schemes. One centralized reader may be present at a field, while multiple low-cost carrier emitters can be placed randomly around a field with scattered sensors. That way, the emitter-to-tag path loss can be statistically reduced, since it will be more likely for a tag to lay close to a carrier emitter. Thus, the overall field coverage can be extended, as more emitters are placed around. Such an architecture can be seen in Fig. 1.2, with multiple carrier emitters and one centralized reader.

It is noted that the prior art rarely considers bistatic architectures and rather focuses on the commercial-standard monostatic reader architectures. An example towards the bistatic direction is [16] which suggests using a single carrier emitter with multiple receiving-only readers (listeners) that cooperate to decode tags simultaneously. That, however, does not lead towards coverage extension but is suggested more as a mechanism for tag collision recovery and interference cancellation. Another example of a receiving-only reader is given in [17], where a monitor for commercial-standard Gen2 RFID tags is presented. However, that work does not derive detectors for the tag-to-reader link, but rather exploits heuristic methods of counting pulse durations to determine the transmitted bits. Moreover, the work is tied to the industry-standard FM0 modulation scheme [7].

# Chapter 2

## Scatter Radio Modules

### 2.1 Setup

The experimental setup used throughout this work is a newest version of the one presented in [11]. For carrier emitting, a WSN-like node operating at the UHF band is used, with software controllable carrier frequency and output power. For the receiving part, a commodity software defined radio (SDR) is utilized for capturing backscatter signals at the UHF band (around 867MHz).<sup>1</sup> The captured signals are processed in software on a host PC with modest processing capabilities and all signal processing is done on MATLAB environment with custom scripts. Finally, the RF tags used for experimentation are based firstly on prototype boards and afterwards on fully custom designs, built from discrete components. It is noted that no readily available RFID transponder chips are utilized. The setup is depicted in Fig. 2.1.

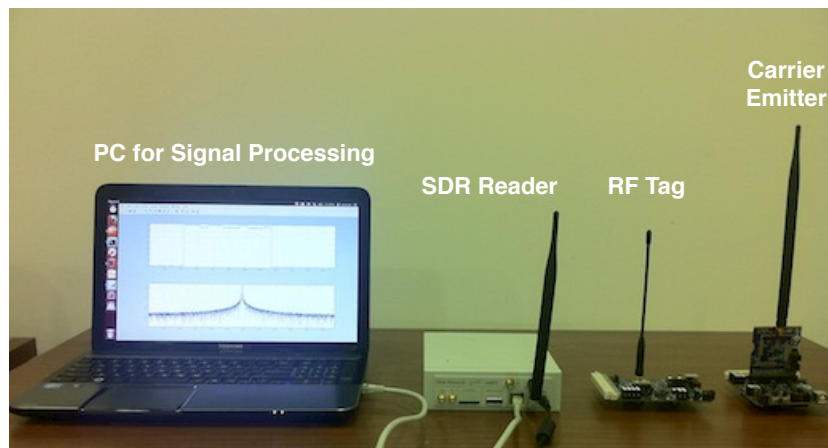


Figure 2.1: Bistatic scatter radio setup.

---

<sup>1</sup>European ISM UHF band.

## 2.2 RF Tag Design

Low-cost, low-power and very high sensor density are the major considerations for RF tag design. Thus, the tags should consist of the very essential components only. Although a fully passive tag design could minimize the cost, a *semi-passive* tag architecture is preferred for increasing the achievable uplink range (tag-to-reader communication) [5,9].

The first tag prototype developed consists of a low-power 8051 microcontroller unit (MCU) evaluation board from Silicon Labs, and a custom printed circuit board (PCB) that enables scatter radio communication (Fig. 2.2). The MCU has a simple instruction set and C language programming capability. For powering the board, a 3V coin-battery in a battery holder is used. Small solar cells with an output voltage of as low as 2V can also be utilized, since the MCU incorporates a DC-to-DC charge pump that fully operates over 1.8V. Sensor connectors and software-controlled LEDs also reside on the MCU evaluation board.

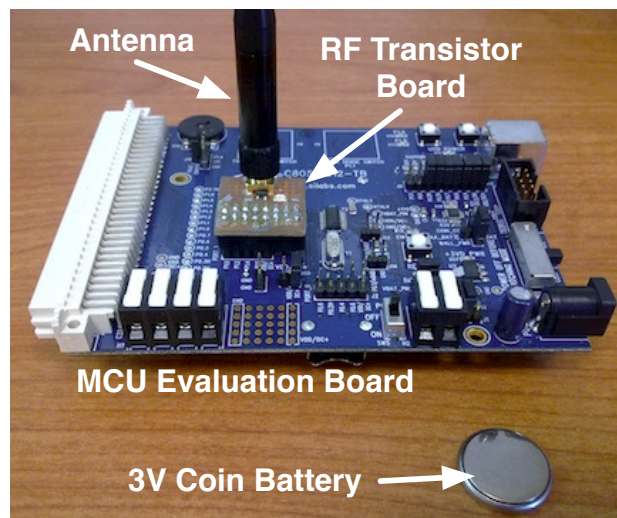


Figure 2.2: Semi-passive tag prototype with its coin battery.

To modulate information, the tag typically terminates its antenna between two loads; in that way, the incident CW is reflected with altered phase and/or amplitude, according to the load that is selected each time. In practice, load switching can be achieved by switching a RF transistor switch

(Fig. 2.3). In that case, when the transistor is switched on, the antenna is short-circuited and any incident wave is scattered back with a negative phase ( $\pi$  radians phase change). Respectively, when the transistor is switched off, the antenna is open-circuited and the incident wave is scattered back intact (i.e. no phase change). A small PCB that plugs directly on the MCU board has been built; it incorporates an RF transistor for load switching and a SMA antenna connector. The latter was preferred over a directly soldered antenna, so that any type of antenna can be tied for experimentation (monopoles, bowties, etc.). The RF transistor is controlled via a MCU pin that supplies the appropriate bias voltage (0V or 3V) for switching the transistor on or off.

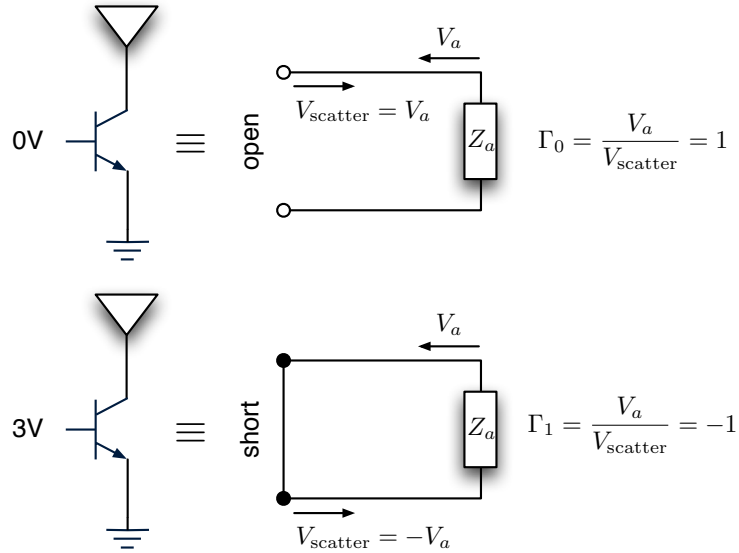


Figure 2.3: Scatter radio modulation with RF transistor.

A full custom tag schematic and PCB layout have also been designed with the Eagle software as a two-layer PCB. This new board has been designed to have a small form-factor, which can be waterproof-packaged and easily attached to plants, along with several types of sensors (e.g. temperature, humidity or soil moisture). The custom design has been kept minimal and comprises of the MCU, the RF transistor modulator, sensor connections, and a LED. This tag is a newer version of the tag built in [18] with a much lower power dissipation. The new tag schematics are given in the Appendix.

## 2.3 Carrier Emitter & Reader

For carrier generation and transmission, a low-cost MCU+embedded radio monolithic chip has been used. The MCU's architecture is based on 8051 and can be used to tune several radio parameters by software, such as carrier frequency, output power, etc. The carrier emitter is essentially a minimal WSN node without sensors or other special circuitry. It operates at the European UHF ISM band (865–868MHz) and has a tuneable output power of up to +13dBm (approx. 20 milliwatts). It is important to note that this carrier emitter is of significantly lower cost compared to the dedicated signal generator used in [11]; moreover it is capable of battery operation. These allow for use of multiple carrier emitters across a field to extend communication range and coverage (see Sec. 1.3). An evaluation board of the carrier emitter used is shown in Fig. 2.4.



Figure 2.4: Carrier emitter evaluation board.

All reception and processing of the backscattered signals is performed at the reader. The reader consists of a receiver tuned at the UHF band to capture backscattered signals, and a series of processing blocks for tag decoding. The reader utilized in this work is software defined, utilizing a low-cost commercial hardware platform, consisting of a UHF RF front-end (RFX900

daughtercard) and fast I/Q analog-to-digital converters (ADCs) (Fig. 2.5). All signal processing is done in MATLAB software running on a PC that hosts the SDR, with custom scripts. This gives the flexibility to control the modulation scheme, data rate, data encoding, etc. The total bandwidth “seen” by the reader can be up to 8 MHz, which is more than enough for low-bitrate scatter radio applications. Modulation-specific processing blocks are described in Chapter 3.

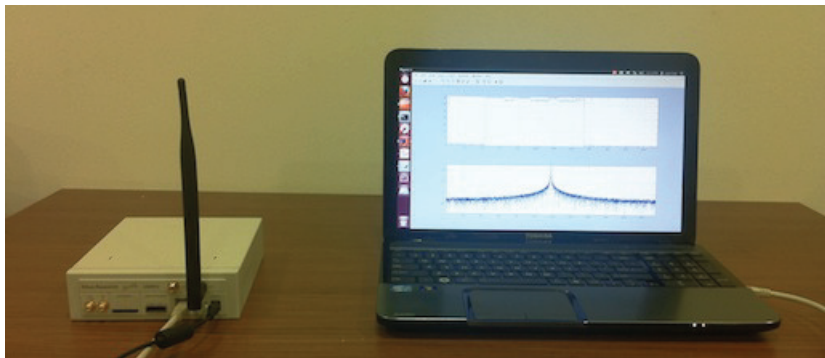


Figure 2.5: SDR Reader consisting of commodity SDR hardware and a PC performing all signal processing.

# Chapter 3

## Bistatic Scatter Radio Links

### 3.1 Signal model

As described in Chapter 1, the bistatic scatter radio system comprises of a carrier emitter, a sensor tag, and a SDR receiver (Fig. 3.1). The carrier emitter illuminates the RF tag with a CW, which is a single-tone, continuous wave at the ultra high frequency (UHF) band. The tag modulates information using its RF transistor front-end and scatters the modulated signal towards the reader. We define the *passband* flat-fading channels depicted in Fig. 3.1:

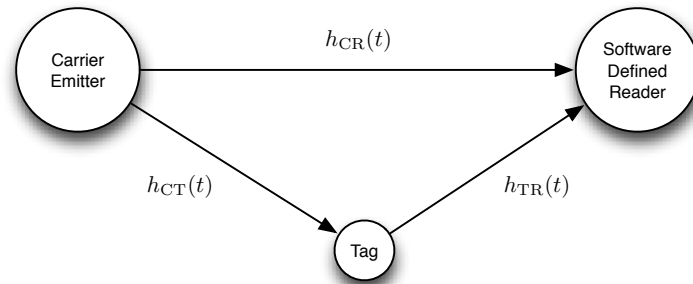


Figure 3.1: Bistatic channel model: carrier emitter is dislocated from the receiving reader and RF tag acts as the signal modulator.

$$h_{CR}(t) = a_{CR} \delta(t - \tau_{CR}), \quad (3.1)$$

$$h_{CT}(t) = a_{CT} \delta(t - \tau_{CT}), \quad (3.2)$$

$$h_{TR}(t) = a_{TR} \delta(t - \tau_{TR}), \quad (3.3)$$

with  $a_* \in \mathbb{R}$ . The corresponding phases they introduce to the propagated signals are:

$$\phi_{\text{CR}} = 2\pi F_c \tau_{\text{CR}}, \quad (3.4)$$

$$\phi_{\text{CT}} = 2\pi F_c \tau_{\text{CT}}, \quad (3.5)$$

$$\phi_{\text{TR}} = 2\pi F_c \tau_{\text{TR}}. \quad (3.6)$$

The carrier emitter transmits a continuous wave of frequency  $F_c$  and power  $P = A^2/2$ :

$$c_{\text{m}}(t) = A \cos(2\pi F_c t), \quad (3.7)$$

where the index “m” indicates that it is a real, passband (i.e. modulated) signal. The RF tag receives from the carrier emitter:

$$c_{\text{m}}(t) * h_{\text{CT}}(t) = A a_{\text{CT}} \cos(2\pi F_c (t - \tau_{\text{CT}})) \quad (3.8)$$

$$= A a_{\text{CT}} \cos(2\pi F_c t - \phi_{\text{CT}}). \quad (3.9)$$

Modulation on the tag is achieved by switching its antenna load between multiple values which correspond to reflection coefficients  $\Gamma_i, i = 0, \dots, M-1$ . The load reflection coefficient changes can be expressed as a function that takes  $M$  distinct values

$$\Gamma(t) \in \{\Gamma_i\}_{i=0}^{M-1}. \quad (3.10)$$

We consider two tag load values, and thus  $\Gamma(t)$  may only take two values:  $\Gamma_0$  and  $\Gamma_1$ .<sup>1</sup> The tag complex baseband signal as a function of time is

$$x(t) \stackrel{\Delta}{=} a_x(t) e^{j\phi_x(t)} = A_s - \Gamma(t), \quad (3.11)$$

where  $A_s$  is a load-independent term related to the antenna *structural mode* [20,21]. It is noted that  $\Gamma(t)$  and  $A_s$  are complex-valued. Then, the amplitude

<sup>1</sup>Recent work has exploited switching between  $M$  load values for higher-order modulation [19].

$a_x(t)$  is

$$a_x(t) \triangleq |A_s - \Gamma(t)|, \quad (3.12)$$

and the phase  $\phi_x(t)$  is

$$\phi_x(t) \triangleq \angle A_s - \Gamma(t), \quad (3.13)$$

i.e. it is the angle of the complex quantity  $A_s - \Gamma(t)$  in radians. The tag scatters back the signal

$$x_m(t) = A a_{CT} s(t) a_x(t) \cos(2\pi F_c t - \phi_{CT} + \phi_x(t)), \quad (3.14)$$

where  $s(t)$  is a scaling term related to the tag scattering efficiency and tag antenna gain at a given direction. The tag efficiency is generally considered time-varying, due to the use of rectifiers on passive tags. For a block of a few bits (e.g. one data packet), however, it may be considered constant. It can be also considered constant in the case of energy assisted (i.e. semipassive) tags where no incoming wave rectification takes place. From now on, we will be considering tag efficiency constant, and will thus simplify  $s(t)$  to  $s$ .

The SDR receiver (reader) receives the superposition of the carrier emitter CW and the backscattered tag signal through channels  $h_{CR}(t)$  and  $h_{TR}(t)$ , respectively:

$$\begin{aligned} y_m(t) = & A [a_{CR} \cos(2\pi F_c t - \phi_{CR}) \\ & + a_{CT} a_{TRS} a_x(t - \tau_{TR}) \cos(2\pi F_c t - \phi_{CT} - \phi_{TR} + \phi_x(t - \tau_{TR}))] + w(t), \end{aligned} \quad (3.15)$$

where  $w(t)$  is band-limited additive Gaussian noise with power spectral density (PSD)

$$S_w(F) = \begin{cases} \frac{N_0}{2}, & |F \pm F_c| \leq W, \\ 0, & \text{elsewhere,} \end{cases} \quad (3.16)$$

where  $2W$  is the passband receiver bandwidth and  $F_c \gg W$ . The reader demodulates the incoming signal with local oscillator (LO) carrier  $F_c + \Delta F$  and phase  $\phi_R$ , and then filters out the high frequency components.  $\Delta F$  is the frequency difference between the emitter and the reader, i.e. it is the carrier frequency offset (CFO). The lowpass in-phase and quadrature components are:

$$I(t) = \text{LPF}\{y_m(t) \cos(2\pi(F_c + \Delta F)t + \phi_R)\}, \quad (3.17)$$

$$Q(t) = \text{LPF}\{-y_m(t) \sin(2\pi(F_c + \Delta F)t + \phi_R)\}. \quad (3.18)$$

After lowpass filtering around  $[-W, W]$ :

$$\begin{aligned} I(t) &= \frac{Aa_{\text{CR}}}{2} \cos(2\pi\Delta Ft + \hat{\phi}_{\text{CR}}) \\ &\quad + \frac{Asa_{\text{CT}}a_{\text{TR}}}{2} a_x(t - \tau_{\text{TR}}) \cos(2\pi\Delta Ft + \hat{\phi}_{\text{CTR}} - \phi_x(t - \tau_{\text{TR}})) + n_I(t), \end{aligned} \quad (3.19)$$

$$\begin{aligned} Q(t) &= -\frac{Aa_{\text{CR}}}{2} \sin(2\pi\Delta Ft + \hat{\phi}_{\text{CR}}) \\ &\quad - \frac{Asa_{\text{CT}}a_{\text{TR}}}{2} a_x(t - \tau_{\text{TR}}) \sin(2\pi\Delta Ft + \hat{\phi}_{\text{CTR}} - \phi_x(t - \tau_{\text{TR}})) + n_Q(t), \end{aligned} \quad (3.20)$$

with

$$\hat{\phi}_{\text{CR}} \triangleq \phi_{\text{CR}} + \phi_R, \quad (3.21)$$

$$\hat{\phi}_{\text{CTR}} \triangleq \phi_{\text{CT}} + \phi_{\text{TR}} + \phi_R. \quad (3.22)$$

The terms  $n_I(t), n_Q(t)$  are lowpass Gaussian noise components with PSD

$$S_{n_I}(F) = S_{n_Q}(F) = \begin{cases} \frac{N_0}{4}, & |F| \leq W, \\ 0, & \text{elsewhere.} \end{cases} \quad (3.23)$$

and variance

$$\sigma_n^2 = \mathbb{E}[n_I^2(t)] = \mathbb{E}[n_Q^2(t)] = \frac{N_0}{4} 2W = \frac{N_0 W}{2}. \quad (3.24)$$

Proof for the above can be found in the Appendix. The complex baseband received signal is

$$y(t) \triangleq I(t) + jQ(t) \quad (3.25)$$

$$= \frac{A}{2} [a_{\text{CR}} e^{-j\hat{\phi}_{\text{CR}}} + a_{\text{CT}} a_{\text{TRS}} x(t - \tau_{\text{TR}}) e^{-j\hat{\phi}_{\text{CTR}}} e^{-j2\pi\Delta F t} + n(t)], \quad (3.26)$$

with  $n(t) = n_I(t) + jn_Q(t)$  complex Gaussian noise, with zero-mean and variance  $\mathbb{E}[|n(t)|^2] = \mathbb{E}[n_I^2(t)] + \mathbb{E}[n_Q^2(t)] = 2\sigma_n^2$ .

Given the extended bit duration, it is assumed that wireless channels between the generator and the reader or the tag, as well as between the tag and the reader, change within a *small* number of consecutive bits, i.e. the channel coherence time spans a limited number of bits. On the contrary, for conventional high bit-rate applications, the channel coherence time spans a significantly larger number of bits. The same holds for the CFO, whose value has significantly changed within a limited number of bits.

## 3.2 Modulation Schemes & Receivers

For the bistatic scatter radio link, two modulation schemes are presented, each with its corresponding processing for sensor data decoding. The first one is based on on-off keying (OOK), which is a popular binary modulation scheme among commercial RFID systems. It is shown that even if a tag modulates information using binary phase shift keying (BPSK), or amplitude shift keying (ASK), or a hybrid of those two, it can be seen as an OOK modulation at the receiver side.<sup>2</sup> OOK is a modulation scheme suitable for

<sup>2</sup>For true BPSK, a semipassive tag has to switch between reflection coefficients  $\Gamma_0 = 1$  and  $\Gamma_1 = -1$ . For ASK, the two reflection coefficients' amplitude values have to differ, but their phases shall remain the same, i.e.  $|\Gamma_0| \neq |\Gamma_1|$ ,  $\angle\Gamma_0 = \angle\Gamma_1$ . For OOK, the tag has to switch between  $\Gamma_0 = 0$  and  $\Gamma_1 = 1$ . In practice, most commercial tags perform a hybrid

the bandwidth-limited regime, while the second scheme presented is more suitable for the power-limited regime and is based on frequency shift keying (FSK). FSK modulation shows some advantages over OOK for scatter radio networks, where extended range, simple multiple access, and increased receiver sensitivity are necessary. A complete comparison of the two schemes is given later in this work.

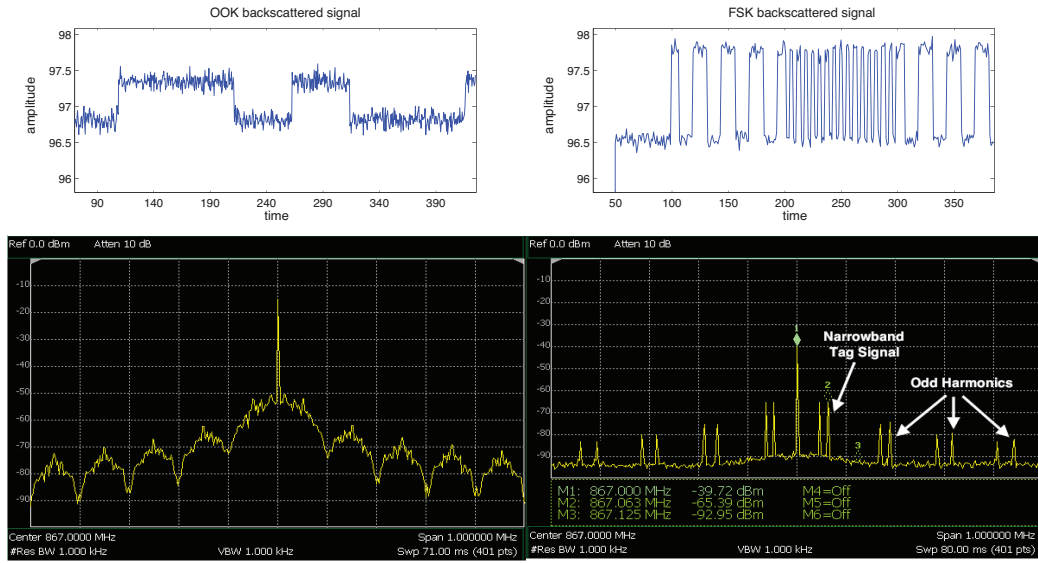


Figure 3.2: Left: Baseband OOK backscattered signal and its corresponding spectrum. Right: Baseband FSK backscattered signal and its corresponding spectrum.

### 3.2.1 OOK

The antenna load's reflection coefficient is  $\Gamma_0$  or  $\Gamma_1$  for bit '0' or bit '1', respectively. Then the baseband backscattered signal of Eq. (3.11) is expressed as:

$$x(t) = \left(A_s - \frac{\Gamma_0 - \Gamma_1}{2}\right) + \frac{\Gamma_0 - \Gamma_1}{2} \sum_{n=0}^{N-1} x_n \Pi(t - nT), \quad (3.27)$$

binary modulation scheme, since they switch between two arbitrary reflection coefficient values that may or may not keep the same amplitude or phase.

where  $x_n \in \{-1, +1\}$  are the  $N$  transmitted bits and  $\Pi(t)$  is a pulse of bit duration  $T$ :

$$\Pi(t) = \begin{cases} 1, & 0 \leq t < T, \\ 0, & \text{elsewhere.} \end{cases} \quad (3.28)$$

The backscattered signal (3.27) can be written as

$$x(t) = m_{\text{dc}} e^{j\theta_{\text{dc}}} + m_{\text{mod}} e^{j\theta_{\text{mod}}} \sum_{n=0}^{N-1} x_n \Pi(t - nT), \quad (3.29)$$

with

$$m_{\text{dc}} = |A_s - (\Gamma_0 + \Gamma_1)/2|, \quad \theta_{\text{dc}} = \angle A_s - (\Gamma_0 + \Gamma_1)/2 \quad (3.30)$$

$$m_{\text{mod}} = |\Gamma_0 - \Gamma_1|/2, \quad \theta_{\text{mod}} = \angle \Gamma_0 - \Gamma_1. \quad (3.31)$$

The SDR receives according to (3.26) and (3.29):

$$y(t) = y_{\text{nl}}(t) + n(t), \quad (3.32)$$

$$= \left[ \hat{m}_{\text{dc}} e^{j\hat{\phi}_{\text{dc}}} + \hat{m}_{\text{mod}} e^{j\hat{\phi}_{\text{mod}}} \sum_{n=0}^{N-1} x_n \Pi(t - \tau_{\text{TR}} - nT) \right] e^{-j2\pi\Delta F t} + n(t), \quad (3.33)$$

with

$$\hat{m}_{\text{dc}} e^{j\hat{\phi}_{\text{dc}}} \triangleq \frac{A}{2} [a_{\text{CR}} e^{-j\hat{\phi}_{\text{CTR}}} + s a_{\text{CT}} a_{\text{TR}} m_{\text{dc}} e^{j(\theta_{\text{dc}} - \hat{\phi}_{\text{CTR}})}], \quad (3.34)$$

$$\hat{m}_{\text{mod}} e^{j\hat{\phi}_{\text{mod}}} \triangleq \frac{A}{2} s a_{\text{CT}} a_{\text{TR}} m_{\text{mod}} e^{j(\theta_{\text{mod}} - \hat{\phi}_{\text{CTR}})}. \quad (3.35)$$

After sampling the baseband signal with sampling period  $T_s$ , the digitized signal is given by

$$y[k] = y(kT_s + \tau_{\text{TR}}) = y_{\text{nl}}[k] + n[k], \quad (3.36)$$

with  $n[k] \sim \mathcal{CN}(0, 2\sigma_n^2)$ .<sup>3</sup>

The term  $y_{\text{nl}}[k]$  refers to the *noiseless* received signal that comprises of a DC component and a modulated component. The DC component comes from the combination of the CW received through the emitter-to-reader channel and an unmodulated component  $m_{\text{dc}}e^{j\theta_{\text{dc}}}$  which is backscattered by the tag. Notice that this noiseless received signal suffers from a CFO term, due to the oscillator inaccuracies on both the carrier emitter and the SDR reader. The CFO causes detector performance loss, and is thus strongly undesired. A way to eliminate the CFO term of the noiseless signal—without estimating it—is by taking the absolute value  $|y_{\text{nl}}(t)|$ . Then the receiver observes the *amplitude* of the received signal which takes two distinct values, according to the binary modulation performed by the tag. Specifically, the complex noiseless samples  $y_{\text{nl}}[k]$  of the (carrier+tag) signal received have amplitude values which are denoted as:

$$s_k \triangleq |y_{\text{nl}}[k]| = \begin{cases} a, & \text{if bit '0'}, \\ b, & \text{if bit '1'}, \end{cases} \quad (3.37)$$

where, without loss of generality, it is assumed that  $a < b$ . In Fig. 3.2-upperleft, a backscattered OOK signal is shown as a function of time. Bit '0' is depicted as a low signal level  $a$  for duration  $kT_s = T$  and bit '1' is shown as a high signal level  $b$  for duration  $T$ . Considering  $a$  as a reference level, it can be removed as an offset. This results in two levels, 0 and  $b - a$ , justifying the OOK terminology.

It is clear that the processing that will take place for the received tag signals is completely non-linear, since it depends on the nonlinear absolute operation. We will now define some useful quantities for the BER performance characterization of the proposed receivers. The carrier-to-noise ratio

---

<sup>3</sup>Notation  $n \sim \mathcal{CN}(0, 2\sigma^2)$  means that  $n = n_r + jn_i$  is complex, circularly symmetric Gaussian, i.e.  $n_r, n_i$  are zero-mean, independent and identically distributed random variables according to Gaussian distribution  $\mathcal{N}(0, \sigma^2)$ .

(CNR) is defined as:

$$\text{CNR} \triangleq \frac{a^2/2}{\mathbb{E}[|n[k]|^2]} L = \frac{a^2}{4\sigma_n^2} L, \quad (3.38)$$

where  $a^2$  is the received carrier power (Fig. 3.2). The division of  $a^2$  by 2 denotes that the carrier is an ‘on-off’ signal, i.e. the carrier generator may transmit a carrier wave, or not.  $L \triangleq T/T_s$  is the oversampling factor, with  $T$  being the symbol duration (i.e. bit duration for binary modulation), and  $T_s$  being the sampling period. The CNR is an important quantity because, in sharp contrast to classic Marconi-type communicators which radiate their own carrier during transmission, the carrier in scatter radio is emitted from a different than the tag terminal. We define the tag signal-to-noise ratio (SNR), *after* the absolute operation, as:

$$\text{SNR} \triangleq \frac{(b-a)^2/2}{\mathbb{E}[|n[k]|^2]} L = \frac{(b-a)^2}{4\sigma_n^2} L. \quad (3.39)$$

Notice that the difference  $b-a$  compared to noise power affects the success in detecting which bit was transmitted. Another useful quantity is introduced, namely the carrier-to-signal ratio (CSR),

$$\text{CSR} \triangleq \frac{\mathcal{P}_c}{\mathcal{P}_b} = \frac{a^2}{(b-a)^2}, \quad (3.40)$$

which indicates the ratio between the received carrier and the useful tag signal. Notice that  $\text{CSR} = \text{CNR}/\text{SNR}$ .

The squared magnitude of the baseband signal  $m_k^2 = |y[k]|^2$ , for given  $s_k \in \{a, b\}$ , is the sum of two squared, independent Gaussians with the same variance and different means; thus,  $m_k^2$  follows a non-central Chi-squared distribution with 2 degrees of freedom and non-centrality parameter  $s_k$  [22].

The absolute operation removes the unknown CFO,

$$|y[k]|^2 = |y_{\text{nl}}[k]|^2 + 2\Re\{y_{\text{nl}}[k] n^*[k]\} + |n[k]|^2. \quad (3.41)$$

Therefore, the receiver can process the CFO-free  $|y_{\text{nl}}[k]|^2$ , along with noise

$|n[k]|^2$  plus another (data-dependent) noise component  $\Re\{y_{nl}[k] n^*[k]\}$ .

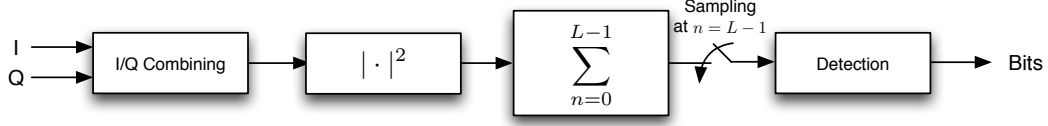


Figure 3.3: Signal processing chain for OOK data.

The squared magnitude  $\{m_k^2\}$  of the received signal is filtered using a square pulse impulse response  $\Pi[k]$ , given by:

$$\Pi[k] = \begin{cases} 1, & 0 \leq k \leq L-1, \\ 0, & \text{otherwise,} \end{cases} \quad (3.42)$$

which has a length of  $L$  taps. The filtered signal is then sampled at the end of each symbol period and each sampled symbol is expressed as:

$$r \triangleq \sum_{k=0}^{L-1} m_k^2 \Pi[L-1-k] = \sum_{k=0}^{L-1} |y[k]|^2. \quad (3.43)$$

Random variable  $r$  is the sum of  $L$  independent, identically distributed non-central Chi-squared random variables, and thus follows a non-central Chi-squared distribution with  $2L$  degrees of freedom; its probability density function (PDF) is given by [23]:

$$f_R(r|s_R, 2L, \sigma_n^2) = \frac{1}{2\sigma_n^2} \left( \frac{r}{s_R^2} \right)^{\frac{L-1}{2}} \exp\left(-\frac{r+s_R^2}{2\sigma_n^2}\right) I_{L-1}\left(\frac{\sqrt{r} s_R}{\sigma_n^2}\right), \quad r \geq 0, \quad (3.44)$$

where  $I_v(\cdot)$  is the  $v$ -th order modified Bessel function of the first kind. The non-centrality parameter  $s_R$  is given by:

$$s_R^2 \triangleq \sum_{k=0}^{L-1} s_k^2 = \begin{cases} L a^2, & \text{if bit '0',} \\ L b^2, & \text{if bit '1'}. \end{cases} \quad (3.45)$$

The cumulative distribution function (CDF) of random variable  $r$  is given

by:

$$F_{R|s_R, 2L, \sigma_n^2}(r) \triangleq \Pr(R \leq r) = 1 - Q_L \left( \frac{s_R}{\sigma_n}, \frac{\sqrt{r}}{\sigma_n} \right), \quad (3.46)$$

where  $Q_M(a, b) = \int_b^\infty x \left(\frac{x}{a}\right)^{M-1} \exp\left(-\frac{x^2+a^2}{2}\right) I_{M-1}(ax) dx$  is the generalized Marcum Q-function [24].

The minimum probability of error detector is needed for the following binary hypothesis problem:

$$\begin{aligned} H_0 : f_{R|H_0}(r|H_0) &= f_R(r|s_a, 2L, \sigma_n^2), & s_a^2 &= L a^2, \\ H_1 : f_{R|H_1}(r|H_1) &= f_R(r|s_b, 2L, \sigma_n^2), & s_b^2 &= L b^2. \end{aligned}$$

For equiprobable hypotheses, the minimum bit error rate (BER) detector is the maximum-likelihood (ML) detector, given by:

$$\begin{aligned} f_{R|H_1}(r|H_1) &\stackrel{H_1}{\geq} f_{R|H_0}(r|H_0) & (3.47) \\ \Leftrightarrow \left(\frac{1}{s_b}\right)^{L-1} \exp\left(-\frac{r_k + s_b^2}{2\sigma_n^2}\right) I_{L-1}\left(\frac{\sqrt{r_k} s_b}{\sigma_n^2}\right) & \\ &\stackrel{H_1}{\geq} \left(\frac{1}{s_a}\right)^{L-1} \exp\left(-\frac{r_k + s_a^2}{2\sigma_n^2}\right) I_{L-1}\left(\frac{\sqrt{r_k} s_a}{\sigma_n^2}\right). \end{aligned}$$

The above ML detector, even though BER-optimal, requires numerical computation of the two  $L-1$ -th order modified Bessel functions of the first kind. For large arguments of the modified Bessel functions  $I_{L-1}(\cdot)$ , the approximation  $I_{L-1}(z) \approx \frac{e^z}{\sqrt{2\pi z}}$  [24] simplifies the above detector to:

$$\begin{aligned} \exp\left(\frac{s_a^2 - s_b^2}{2\sigma_n^2}\right) \frac{\exp(\sqrt{r} s_b/\sigma_n^2)}{\sqrt{2\pi\sqrt{r} s_b/\sigma_n^2}} &\stackrel{H_1}{\geq} \left(\frac{s_b}{s_a}\right)^{L-1} \frac{\exp(\sqrt{r} s_a/\sigma_n^2)}{\sqrt{2\pi\sqrt{r} s_a/\sigma_n^2}} \\ \Leftrightarrow r &\stackrel{H_1}{\geq} \left[ \frac{\sigma_n^2}{s_b - s_a} \left(L - \frac{1}{2}\right) \ln(s_b/s_a) + \frac{s_b + s_a}{2} \right]^2 \triangleq \eta_1, \end{aligned} \quad (3.48)$$

where we have taken  $s_b > s_a$  into account. The above detector requires estimation of the parameters  $a, b, \sigma_n^2$ . It will be shown in the numerical results that the BER performance of the above detector coincides with the

ML detector performance for high CSR values, which is the typical case in scatter radio.

A simple (heuristic) detector is also tested, in order to bypass the need for Bessel function computation as well as the need for estimation of parameters  $a, b, \sigma^2$ . This appealing detector calculates the average value of a received preamble, other than the information data, and utilizes such value as the decision threshold. The heuristic detector is given by:

$$r \stackrel{H_1}{\geq} \frac{1}{N_p} \sum_{i=0}^{N_p-1} \tilde{r}_i \triangleq \eta_2, \quad (3.49)$$

where  $\tilde{r}_i$ ,  $i = 0, \dots, N_p - 1$  are the  $N_p$  preamble symbols (which are independent of the data) after filtering with  $\Pi[k]$  and sampling. The above heuristic detector requires the calculation of the above threshold only, and no further estimation of the parameters  $a, b, \sigma^2$ . Notice however, that the number  $N_p$  cannot be made arbitrarily large, since in that case the channel values (and hence parameters  $a, b$ ) may have changed.

The above processing, summarized in Fig. 3.3, as well as the described detectors, assume symbol synchronization, which can be implemented using correlation with a sequence of known bits in the preamble. Moreover, the receiver needs to determine whether the information bits have been flipped due to channel conditions (i.e. high level has become low and vice versa). This is managed through comparison of the detected preamble bits with the a priori known bit sequence.

### 3.2.2 FSK

In FSK, the tag switches between two distinct reflection coefficient values  $\Gamma_0, \Gamma_1$  with different rates  $F_i$  for corresponding bits  $i = 0, 1$  (also called subcarrier frequencies). To ensure orthogonality in noncoherent FSK, the spacing between the two subcarrier frequencies is  $|F_1 - F_0| = k\frac{1}{T}$ ,  $k \in \mathbb{N}$ , where  $T$  is the bit duration. For each bit, this results in a baseband backscattered

waveform that can be written as

$$x(t) = \left(A_s - \frac{\Gamma_0 + \Gamma_1}{2}\right) + \frac{\Gamma_0 - \Gamma_1}{2} b_i(t), \quad i = 0, 1, \quad (3.50)$$

where  $b_i(t)$  represents a 50% duty cycle square waveform of frequency  $F_i$ , random initial phase  $\Phi \sim \mathcal{U}[0, 2\pi)$  and amplitude 1 (i.e. level switches between  $-1$  and  $+1$ ):

$$b_i(t) = \frac{4}{\pi} \sum_{k=0}^{+\infty} \frac{1}{2k+1} \cos[(2k+1)(2\pi F_i t + \Phi)]. \quad (3.51)$$

Because of the limited receiver bandwidth, we consider that  $3F_i \gg W$ . Keeping only the fundamental frequency component of  $b_i(t)$  and substituting it in (3.50), the (filtered) tag complex baseband backscattered waveform is written as

$$\tilde{x}(t) = \left(A_s - \frac{\Gamma_0 + \Gamma_1}{2}\right) + \frac{\Gamma_0 - \Gamma_1}{2} \frac{4}{\pi} \cos(2\pi F_i t + \Phi) \quad (3.52)$$

$$= m_{\text{dc}} e^{j\theta_{\text{dc}}} + m_{\text{mod}} \cos(2\pi F_i t + \Phi) e^{j\theta_{\text{mod}}}, \quad (3.53)$$

with

$$m_{\text{dc}} = |A_s - (\Gamma_0 + \Gamma_1)/2|, \quad \theta_{\text{dc}} = \angle A_s - (\Gamma_0 + \Gamma_1)/2 \quad (3.54)$$

$$m_{\text{mod}} = 2|\Gamma_0 - \Gamma_1|/\pi, \quad \theta_{\text{mod}} = \angle \Gamma_0 - \Gamma_1. \quad (3.55)$$

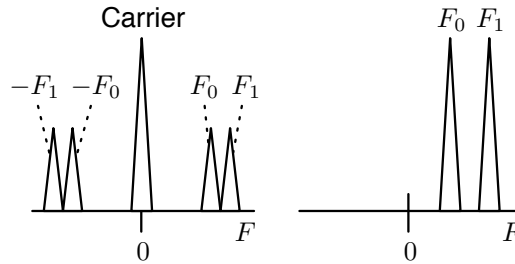


Figure 3.4: Complex baseband spectrum for scatter radio FSK (left) and ‘classic’ FSK (right). Two subcarriers per frequency exist in scatter radio FSK, in contrast with classic FSK.

According to Eq. (3.26), the SDR receives:

$$y(t) = \left[ \hat{m}_{\text{dc}} e^{j\hat{\phi}_{\text{dc}}} + \hat{m}_{\text{mod}} \cos(2\pi F_i t + \Phi') e^{j\hat{\phi}_{\text{mod}}} \right] e^{-j2\pi\Delta F t} + n(t), \quad (3.56)$$

with

$$\hat{m}_{\text{dc}} e^{j\hat{\phi}_{\text{dc}}} \triangleq \frac{A}{2} [a_{\text{CR}} e^{-j\hat{\phi}_{\text{CR}}} + sa_{\text{CT}} a_{\text{TR}} m_{\text{dc}} e^{j(\theta_{\text{dc}} - \hat{\phi}_{\text{CTR}})}], \quad (3.57)$$

$$\hat{m}_{\text{mod}} e^{j\hat{\phi}_{\text{mod}}} \triangleq \frac{A}{2} sa_{\text{CT}} a_{\text{TR}} m_{\text{mod}} e^{j(\theta_{\text{mod}} - \hat{\phi}_{\text{CTR}})}, \quad (3.58)$$

$$\Phi' \triangleq \Phi - 2\pi F_i \tau_{\text{TR}}. \quad (3.59)$$

In Fig. 3.4 the spectrum of the complex baseband is shown, for scatter radio FSK and for ‘classic’ FSK. Notice that because the tag modulation occurs directly at passband, *two* subcarriers appear for each frequency  $F_i$ , one at the positive semiaxis and one at the negative (Fig. 3.4-left). In contrast, for a classic active FSK transmitter, only one subcarrier appears for each frequency (Fig. 3.4-right). For the latter, an FSK receiver is used which correlates against frequencies  $F_0$  and  $F_1$  for signal demodulation [25]. However, if the same receiver is applied for scatter radio FSK, only the subcarriers at frequencies  $F_0$  and  $F_1$  will be considered, leaving out  $-F_0$  and  $-F_1$ . This results in a 3dB loss of information and degraded receiver performance. The above show that a classic FSK receiver is not applicable in scatter radio, since it does not account for the correct signal model. Thus, a different processing chain has to be designed for successful signal demodulation.

Assuming no CFO (i.e.  $\Delta F = 0$ ), the received waveform is

$$y(t) = \hat{m}_{\text{dc}} e^{j\hat{\phi}_{\text{dc}}} + \hat{m}_{\text{mod}} \cos(2\pi F_i t + \Phi') e^{j\hat{\phi}_{\text{mod}}} + n(t). \quad (3.60)$$

After sampling with sampling period  $T_s$ , the baseband digitized signal is

$$y[k] = y(kT_s) = \hat{m}_{\text{dc}} e^{j\hat{\phi}_{\text{dc}}} + \hat{m}_{\text{mod}} \cos(2\pi F_i kT_s + \Phi') e^{j\hat{\phi}_{\text{mod}}} + n[k], \quad (3.61)$$

with  $n[k] \sim \mathcal{CN}(0, 2\sigma_n^2)$ . The DC term  $\hat{m}_{\text{dc}} e^{j\hat{\phi}_{\text{dc}}}$  does not contribute any information on the transmitted data, and so it can be blocked using a DC-

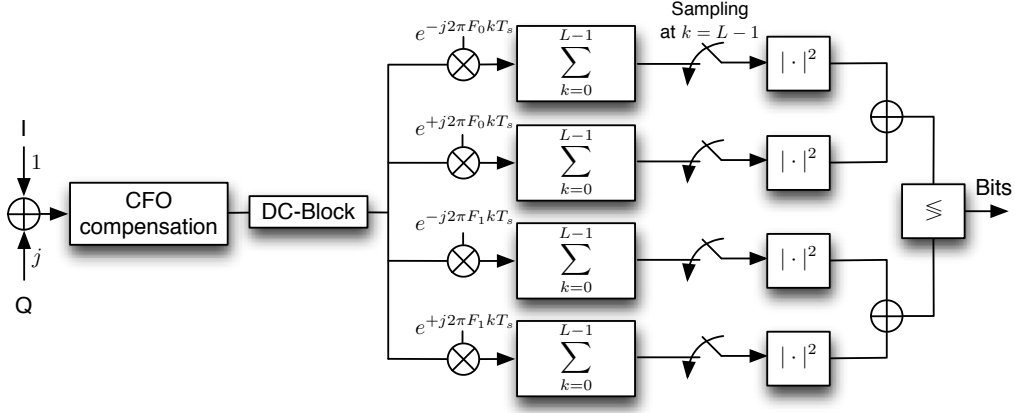


Figure 3.5: FSK signal processing chain. After CFO compensation and DC-blocking, the complex baseband signal is correlated against  $\pm F_0, \pm F_1$  for  $L$  samples, which correspond to one bit duration  $T$ . Then, the correlator outputs are sampled and detection is performed on the samples.

blocking filter.<sup>4</sup> After DC-blocking, the waveform is

$$\tilde{y}[k] = \hat{m}_{\text{mod}} \cos(2\pi F_i k T_s + \Phi') e^{j\hat{\phi}_3} + n[k]. \quad (3.62)$$

The received SNR at baseband is

$$\text{SNR} \triangleq \frac{\hat{m}_{\text{mod}}^2/2}{\mathbb{E}[|n[k]|^2]} L = \frac{\hat{m}_{\text{mod}}^2}{4\sigma_n^2} L. \quad (3.63)$$

Observing (3.62), we can notice that a ‘classic’ non-coherent FSK demodulator (envelope detector) cannot be directly applied for demodulating the received signal, due to the presence of the unknown term  $e^{j\hat{\phi}_{\text{mod}}}$ . Equation (3.62) can be rewritten as

$$\tilde{y}[k] = \frac{\hat{m}_{\text{mod}}}{2} e^{j(2\pi F_i k T_s + \Phi' + \hat{\phi}_3)} + \frac{\hat{m}_{\text{mod}}}{2} e^{-j(2\pi F_i k T_s + \Phi' - \hat{\phi}_3)} + n[k]. \quad (3.64)$$

Thus the received signal is a sum of two complex exponentials, of frequencies  $F_i$  and  $-F_i$ , respectively, and unknown phases  $(\Phi' + \hat{\phi}_{\text{mod}})$  and  $(-\Phi' + \hat{\phi}_{\text{mod}})$ . Any two exponentials with frequencies  $\pm F_0, \pm F_1$  are orthogonal (proof is

<sup>4</sup>DC-blocking can be implemented by estimation and removal of the received signal’s mean value  $\mathcal{E}\{y(t)\}$ .

given in the Appendix), and a correlation demodulator that exploits the orthogonality can be used for demodulation. For one bit duration  $T$ , a bank of correlation demodulators processes  $L = T/T_s$  samples and yields the statistics

$$r_0^+ = \sum_{k=0}^{L-1} \tilde{y}[k] e^{-j2\pi F_0 k T_s} \quad (3.65)$$

$$\begin{aligned} &= \frac{\hat{m}_{\text{mod}}}{2} \sum_{k=0}^{L-1} e^{j(2\pi(F_i - F_0)k T_s + \Phi' + \hat{\phi}_{\text{mod}})} \\ &\quad + \underbrace{\frac{\hat{m}_{\text{mod}}}{2} \sum_{k=0}^{L-1} e^{-j(2\pi(F_i + F_0)k T_s + \Phi' - \hat{\phi}_{\text{mod}})}}_{\approx 0} + \sum_{k=0}^{L-1} n'[k] \\ &= \frac{\hat{m}_{\text{mod}}}{2} \sum_{k=0}^{L-1} e^{+j(2\pi(F_i - F_0)k T_s + \Phi' + \hat{\phi}_{\text{mod}})} + n_0^+. \end{aligned} \quad (3.66)$$

Notice that the sum of the “fast” exponential with frequency  $F_i + F_0$  is approximated by zero. Also, notice that the noise term  $n'[k] \triangleq n[k] e^{\pm j2\pi F_i k T_s}$  follows the same distribution with  $n[k]$ , i.e. it is circularly-symmetric Gaussian. The other correlator statistics are:

$$r_0^- = \sum_{k=0}^{L-1} \tilde{y}[k] e^{+j2\pi F_0 k T_s} = \frac{\hat{m}_{\text{mod}}}{2} \sum_{k=0}^{L-1} e^{-j(2\pi(F_i - F_0)k T_s + \Phi' - \hat{\phi}_{\text{mod}})} + n_0^- \quad (3.67)$$

$$r_1^+ = \sum_{k=0}^{L-1} \tilde{y}[k] e^{-j2\pi F_1 k T_s} = \frac{\hat{m}_{\text{mod}}}{2} \sum_{k=0}^{L-1} e^{+j(2\pi(F_i - F_1)k T_s + \Phi' + \hat{\phi}_{\text{mod}})} + n_1^+ \quad (3.68)$$

$$r_1^- = \sum_{k=0}^{L-1} \tilde{y}[k] e^{+j2\pi F_1 k T_s} = \frac{\hat{m}_{\text{mod}}}{2} \sum_{k=0}^{L-1} e^{-j(2\pi(F_i - F_1)k T_s + \Phi' - \hat{\phi}_{\text{mod}})} + n_1^- \quad (3.69)$$

When bit ‘1’ is transmitted, the received signal has frequency  $F_1$  and thus, the statistics are

$$r_0^+ = n_0^+, \quad r_1^+ = \frac{\hat{m}_{\text{mod}} L}{2} e^{+j(\Phi' + \hat{\phi}_{\text{mod}})} + n_1^+ \quad (3.70)$$

$$r_0^- = n_0^-, \quad r_1^- = \frac{\hat{m}_{\text{mod}} L}{2} e^{-j(\Phi' - \hat{\phi}_{\text{mod}})} + n_1^- \quad (3.71)$$

On the contrary, when bit ‘0’ is transmitted, the received signal has frequency  $F_0$  and thus, the statistics are

$$r_0^+ = \frac{\hat{m}_{\text{mod}} L}{2} e^{+j(\Phi' + \hat{\phi}_{\text{mod}})} + n_0^+, \quad r_1^+ = n_1^+ \quad (3.72)$$

$$r_0^- = \frac{\hat{m}_{\text{mod}} L}{2} e^{-j(\Phi' - \hat{\phi}_{\text{mod}})} + n_0^-, \quad r_1^- = n_1^- \quad (3.73)$$

Exploiting the statistics at the output of the demodulator, we make use of the detector

$$z_1 \triangleq |r_1^+|^2 + |r_1^-|^2 \stackrel{H_1}{\geq} |r_0^+|^2 + |r_0^-|^2 \triangleq z_0. \quad (3.74)$$

### 3.2.3 Carrier Recovery

Consider (3.56) with a non-zero CFO  $\Delta F$ . Then  $y(t)$  will be a signal of frequency  $\pm F_0 + \Delta F$  or  $\pm F_1 + \Delta F$ ; thus it can not be directly correlated against the frequencies  $\pm F_0$  and  $\pm F_1$ . The CFO has to be compensated for successful demodulation and detection. For a *limited* number of bits, where the CFO may be considered static, a per-packet CFO estimation can be achieved using fast fourier transform (FFT) techniques. The periodogram of each packet is calculated with a high frequency resolution  $dF \triangleq F_s/N_F$ , where  $N_F$  is the number of FFT points, such that  $dF \ll 1/T$ . The CFO is estimated by finding the periodogram peak (which corresponds to the transmitted carrier), and is cancelled out by shifting the periodogram to DC. It is noted that for ultra low-bitrate scenarios where  $T$  is maximized,  $N_F$  has to be large for achieving a high frequency resolution. This requires a long processing time, which may be prohibiting in some scenarios.

# Chapter 4

## Performance

### 4.1 BER Performance

#### 4.1.1 OOK

BER calculation for the approximate, high-CSR detector of Eq. (3.48) is given by:

$$\begin{aligned}\Pr(e_{\text{approx}}) &= \frac{1}{2} \Pr(e|H_1) + \frac{1}{2} \Pr(e|H_0) \\ &= \frac{1}{2} \Pr(R < \eta_1|H_1) + \frac{1}{2} \Pr(R \geq \eta_1|H_0) \\ &= \frac{1}{2} F_{R|s_b, 2L, \sigma_n^2}(\eta_1) + \frac{1}{2} (1 - F_{R|s_a, 2L, \sigma_n^2}(\eta_1)) \\ &= \frac{1}{2} - \frac{1}{2} Q_L \left( \frac{s_b}{\sigma_n}, \frac{\sqrt{\eta_1}}{\sigma_n} \right) + \frac{1}{2} Q_L \left( \frac{s_a}{\sigma_n}, \frac{\sqrt{\eta_1}}{\sigma_n} \right).\end{aligned}\quad (4.1)$$

Similarly, BER for the heuristic detector is given by:

$$\Pr(e_{\text{heuristic}}) = \frac{1}{2} \Pr(R < \eta_2|H_1) + \frac{1}{2} \Pr(R \geq \eta_2|H_0). \quad (4.2)$$

Notice that  $\eta_2$  is preamble-dependent, and therefore, is a random threshold. When the threshold is based on  $N$  equiprobable '0's and '1's, it can be written in the following form:

$$\eta_2 = \sum_{i=0}^{N_p/2-1} \sum_{l=0}^{L-1} (X_{I,i,l}^2 + X_{Q,i,l}^2) + \sum_{i=N_p/2}^{N_p-1} \sum_{l=0}^{L-1} (X_{I,i,l}^2 + X_{Q,i,l}^2), \quad (4.3)$$

with

$$\begin{aligned} X_{I,i,l} &\sim \mathcal{N}(\Re\{y_a\}/\sqrt{N_p}, \sigma_n^2/N_p), \quad i = 0, \dots, N_p/2 - 1, \forall l, \\ X_{I,i,l} &\sim \mathcal{N}(\Re\{y_b\}/\sqrt{N_p}, \sigma_n^2/N_p), \quad i = N_p/2, \dots, N_p - 1, \forall l, \\ X_{Q,i,l} &\sim \mathcal{N}(\Im\{y_a\}/\sqrt{N_p}, \sigma_n^2/N_p), \quad i = 0, \dots, N_p/2 - 1, \forall l, \\ X_{Q,i,l} &\sim \mathcal{N}(\Im\{y_b\}/\sqrt{N_p}, \sigma_n^2/N_p), \quad i = N_p/2, \dots, N_p - 1, \forall l. \end{aligned}$$

$\mathcal{N}(\mu_i, \sigma_i^2)$  denotes the (real) normal pdf, with (real) mean  $\mu_i$  and variance  $\sigma_i^2$  and  $y_a, y_b$  denote the values of  $y_{nl}$  when bit ‘0’ or bit ‘1’ is transmitted, respectively. The above also assume that  $N_p$  is an even number. Then,  $\eta_2$  follows the non-central Chi-squared distribution with  $2N_pL$  degrees of freedom and non-centrality parameter  $s_{\eta_2}$  given by:

$$s_{\eta_2}^2 = L \frac{a^2 + b^2}{2}, \quad (4.4)$$

which is independent of  $N_p$ . Thus, the pdf of  $\eta_2$  is given by:

$$\begin{aligned} f_{\eta_2}(\eta_2 | s_{\eta_2}, 2N_pL, \sigma_{\eta_2}^2) &= \frac{1}{2\sigma_{\eta_2}^2} \left( \frac{\eta_2}{s_{\eta_2}^2} \right)^{\frac{N_pL-1}{2}} \exp\left(-\frac{\eta_2 + s_{\eta_2}^2}{2\sigma_{\eta_2}^2}\right) \\ &\times I_{N_pL-1} \left( \frac{\sqrt{\eta_2} s_{\eta_2}}{\sigma_{\eta_2}^2} \right), \quad \eta_2 \geq 0, \end{aligned} \quad (4.5)$$

where  $\sigma_{\eta_2}^2 = \sigma_n^2/N_p$ . We can now calculate the probabilities  $\Pr(R < \eta_2 | H_1)$  and  $\Pr(R \geq \eta_2 | H_0)$  using the law of iterated expectation:

$$\begin{aligned} \Pr(R < \eta_2 | H_1) &= \mathbb{E}_{\eta_2}[\Pr(R < \eta_2 | H_1, \eta_2)] \\ &= 1 - \int_0^\infty Q_L \left( \frac{s_b}{\sigma_n}, \frac{\sqrt{\eta_2}}{\sigma_n} \right) f_{\eta_2}(\eta_2 | s_{\eta_2}, 2N_pL, \sigma_{\eta_2}^2) d\eta_2. \end{aligned} \quad (4.6)$$

Similarly,

$$\begin{aligned} \Pr(R \geq \eta_2 | H_0) &= \mathbb{E}_{\eta_2}[\Pr(R > \eta_2 | H_0, \eta_2)] \\ &= \int_0^\infty Q_L \left( \frac{s_a}{\sigma_n}, \frac{\sqrt{\eta_2}}{\sigma_n} \right) f_{\eta_2}(\eta_2 | s_{\eta_2}, 2N_pL, \sigma_{\eta_2}^2) d\eta_2. \end{aligned} \quad (4.7)$$

Substituting the two above terms in (4.2), the BER of the heuristic detector becomes:

$$\Pr(e_{\text{heuristic}}) = \frac{1}{2} - \frac{1}{2} \frac{1}{\eta_2} \mathbb{E} \left[ Q_L \left( \frac{s_b}{\sigma_n}, \frac{\sqrt{\eta_2}}{\sigma_n} \right) - Q_L \left( \frac{s_a}{\sigma_n}, \frac{\sqrt{\eta_2}}{\sigma_n} \right) \right]. \quad (4.8)$$

Fig. 4.1 shows the performance of the approximate-ML detector of Eq. (3.48). SNR and CSR quantities follow the definitions of Section 3.2.1. It can be seen that analysis matches simulation results. More importantly, for large SNR values the performance of the approximate detector coincides with the performance of the optimal ML detector, even for low CSR value of 0 dB. For higher CSR values, on the order of 10 dB, the performance gap between the two detectors is reduced, even for low SNR values. This is important, since, in practical setups, the calculation of the respective Bessel function may not be practical. Thus, it is concluded that the approximate detector of Eq. (3.48) is near-optimal. It is also seen that for a given SNR value, the increase in CSR (and thus in CNR also) improves BER performance for the particular detector.

That is an interesting result which directs optimization of the carrier power scattered from the tag towards the receiver and it is in sharp contrast to conventional tag design principles applied so far, that aim to optimize SNR only. Thus, tag design should aim to maximize not only SNR but also CNR (or CSR), for the proposed detector. Notice however, that performance for CSR values over 20dB is not significantly improved (as opposed to CSR values between 0 and 10 dB).

Fig. 4.2 depicts the BER performance of the heuristic detector with analytic as well as simulation results, which perfectly match. It is shown that a higher CSR value of 20 dB improves performance, compared to CSR of 0 dB, for the same reasons as in the approx-ML detector. It is re-affirmed that tag design should not only maximize SNR values (namely the difference  $b - a$ ) but also CNR (the values  $a, b$ , and respectively the CSR), when receiving architectures of this work are planned. Practical ways to design tags that adhere to the above design rules (both SNR and CNR maximization) can be found in [21].

Fig. 4.3 compares the near-optimal, approximate ML detector with the heuristic detector, based on their BER performance. It can be seen that for larger values of the CSR, the heuristic detector approaches the performance of the near-optimal, with a performance penalty of less than 0.5 dB. The advantage of the heuristic detector is its simple threshold calculation, which does not require knowledge of the noise variance or the values  $a, b$ , and can be acquired using a series of pilot symbols, provided that the channel will not change during the detection (i.e. the threshold will be estimated on preamble bits and utilized on data under the same channel conditions).

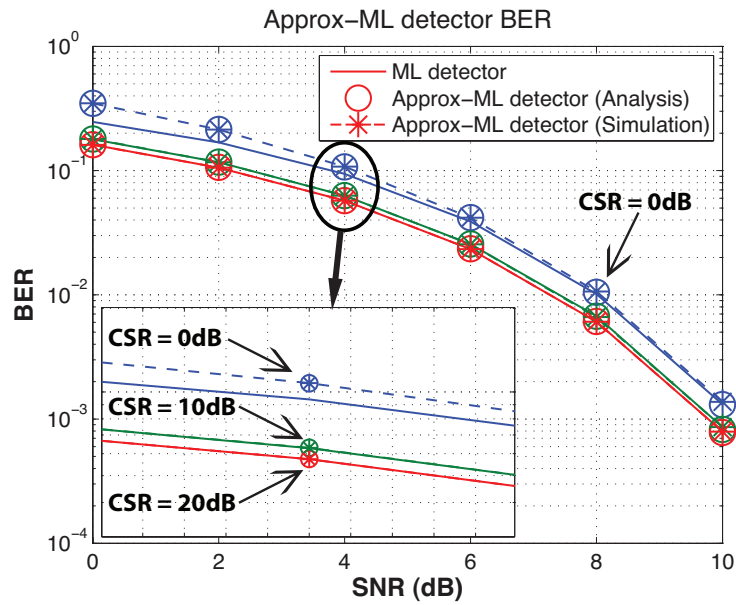


Figure 4.1: Bit error rate for OOK ML and the approx-ML detector, with  $L = 10$ .

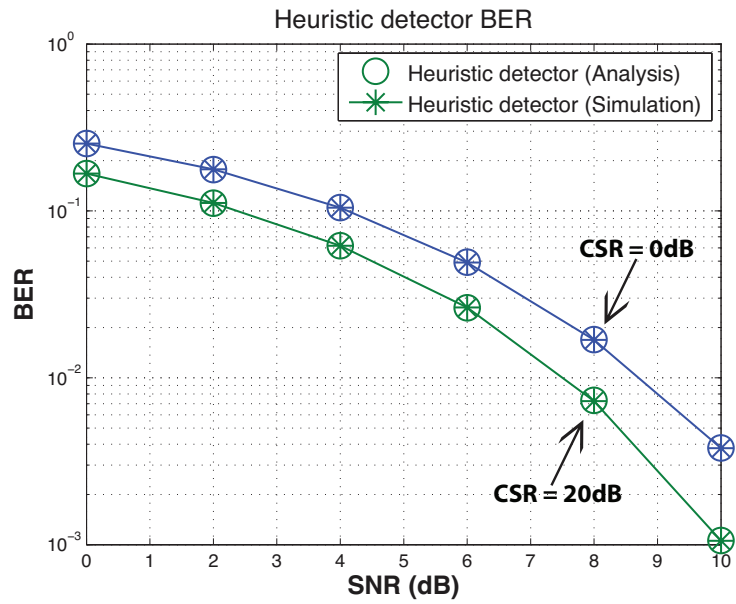


Figure 4.2: Bit error rate of the OOK heuristic detector, with  $L = 10$ .

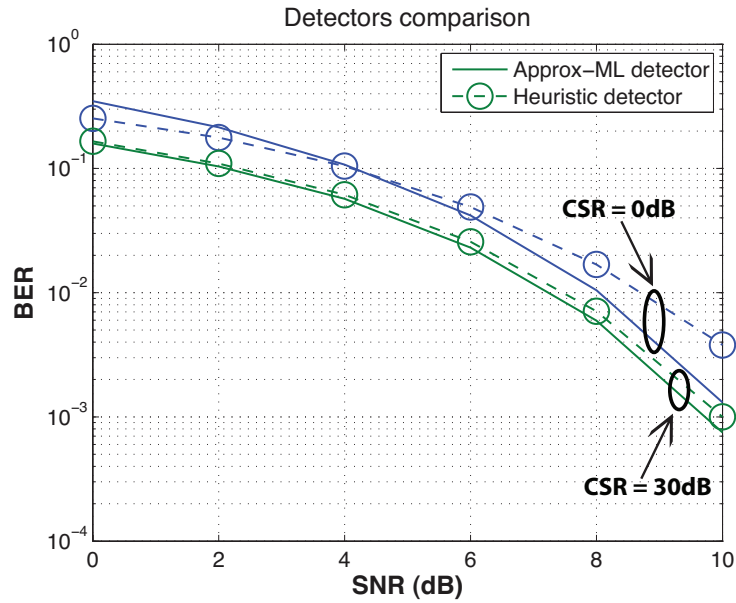


Figure 4.3: Comparison of OOK approx-ML and heuristic detectors.

### 4.1.2 FSK

Under  $H_1$  (bit ‘1’ transmitted) the statistics at the correlator outputs are distributed as shown below (proof is omitted for the Appendix):

$$r_0^+ \sim \mathcal{CN}(0, 2\sigma_n^2 L) \quad (4.9)$$

$$r_0^- \sim \mathcal{CN}(0, 2\sigma_n^2 L) \quad (4.10)$$

$$r_1^+ \sim \mathcal{CN}\left(\frac{\hat{m}_{\text{mod}} L}{2} e^{-j(\Phi' - \hat{\phi}_{\text{mod}})}, 2\sigma_n^2 L\right) \quad (4.11)$$

$$r_1^- \sim \mathcal{CN}\left(\frac{\hat{m}_{\text{mod}} L}{2} e^{-j(\Phi' - \hat{\phi}_{\text{mod}})}, 2\sigma_n^2 L\right) \quad (4.12)$$

Then  $z_0 = |r_0^+|^2 + |r_0^-|^2$  is the sum of 4 squared zero-mean gaussian random variables, each with variance  $\sigma^2 = \sigma_n^2 L$ . Thus  $z_0$  follows a Chi-squared distribution with 4 degrees of freedom [23]:

$$f_{z_0}(z_0|\sigma^2, H_1) = \frac{z_0}{4\sigma^4} \exp\left\{-\frac{z_0}{2\sigma^2}\right\}, \quad z_0 \geq 0 \quad (4.13)$$

$$F_{z_0}(z_0|\sigma^2, H_1) = 1 - \exp\left\{-\frac{z_0}{2\sigma^2}\right\} \left(1 + \frac{z_0}{2\sigma^2}\right). \quad (4.14)$$

The random variable  $z_1 = |r_1^+|^2 + |r_1^-|^2$  is the sum of 4 squared non-zero-mean gaussians random variables, each with variance  $\sigma^2 = \sigma_n^2 L$ . Then  $z_1$  follows a non-central Chi-squared distribution with 4 degrees of freedom. We determine the non-centrality parameter  $s^2$  as follows:

$$s^2 = \left| \frac{\hat{m}_{\text{mod}} L}{2} e^{+j(\Phi' + \hat{\phi}_{\text{mod}})} \right|^2 + \left| \frac{\hat{m}_{\text{mod}} L}{2} e^{-j(\Phi' - \hat{\phi}_{\text{mod}})} \right|^2 = \frac{\hat{m}_{\text{mod}}^2 L^2}{2}. \quad (4.15)$$

The PDF and CDF of  $z_1$  are:

$$f_{z_1}(z_1|s^2, \sigma^2, H_1) = \frac{\sqrt{z_1}}{2\sigma^2 s} \exp\left\{-\frac{z_1 + s^2}{2\sigma^2}\right\} I_1\left(\sqrt{z_1} \frac{s}{\sigma^2}\right), \quad (4.16)$$

$$F_{z_1}(z_1|s^2, \sigma^2, H_1) = 1 - Q_2\left(\frac{s}{\sigma}, \frac{\sqrt{z_1}}{\sigma}\right), \quad z_1 \geq 0. \quad (4.17)$$

The probability of correct decision under  $H_1$  is

$$\Pr(c|H_1) = \Pr(z_0 \leq z_1|H_1) = \quad (4.18)$$

$$\begin{aligned} &= \mathbb{E}_{z_1}[\Pr(z_0 \leq z_1|z_1, H_1)] = \mathbb{E}_{z_1}[F_{z_0|H_1}(z_1|H_1)] \\ &= \int_0^\infty F_{z_0|H_1}(z_1|H_1) f_{z_1|H_1}(z_1|s^2, \sigma^2, H_1) dz_1 \end{aligned} \quad (4.19)$$

Then the probability of error is

$$\Pr(e) = \Pr(e|H_0) = \Pr(e|H_1) = 1 - \Pr(c|H_1). \quad (4.20)$$

The probability of error for scatter radio FSK is shown in Fig. 4.4. The SNR follows the definition of Section 3.2.2. Analysis BER of Eq. (4.20) perfectly matches with simulation, with no CFO between the carrier emitter and the receiver. Next, we characterize the performance of the FSK receiver in the presence of CFO. According to Section 3.2.3, a strong DC term has to be received for successful CFO estimation (Eq. (3.54)). In most scenarios, a strong carrier will be available at the receiver from the emitter-to-reader path (Fig. 3.1), and thus carrier recovery will be successful. However, in the case of emitter-to-reader path blockage (i.e.  $a_{CR} = 0$ ), no DC component from the emitter will be available at the reader. Then the only factor that will contribute a DC to the reader will be the unmodulated carrier reflected by the tag due to the antenna *structural* mode.

To minimize BER, the condition  $|\Gamma_0 - \Gamma_1| = 2$  must hold for semipassive tags, as stated in [21]. Without loss of generality, the values  $\Gamma_0 = 1$  and  $\Gamma_1 = -1$  are chosen for the simulations. Recall from Eq. (3.54) that the backscattered DC amplitude is  $|A_s - (\Gamma_0 + \Gamma_1)/2|$ . For the *specific* value pair, the DC will relate directly to  $|A_s|$ , which will determine the backscattered carrier power. To show the necessity of tag design with respect to  $A_s$ , several values of  $A_s$  are tested; the values are  $A_s = 0.6047 + j0.5042$  with  $|A_s| \approx 0.78$ ,  $A_s = 0.2954 - j0.0524$  with  $|A_s| = 0.3$ , and  $A_s = 0.1593 - j0.1209$  with  $|A_s| = 0.2$ . It can be seen that as  $|A_s|$  grows, the BER drops faster and approaches the theoretical curve, due to the higher estimation accuracy. This essentially

suggests that the antenna structural mode is an important parameter to look after during tag design *along* with the pair of  $\Gamma_0, \Gamma_1$  values. For the proposed FSK receiver, the tag designer should try to maximize  $|A_s - (\Gamma_0 + \Gamma_1)/2|$ . This could be achieved by either choosing appropriate  $\Gamma$ -values for a given  $A_s$  value, or by designing an antenna with an appropriate  $A_s$  value for a given pair of  $\Gamma_0, \Gamma_1$ . In either case, it is directed that antenna parameters and antenna load values should be taken *jointly* into account to maximize the receiver's BER performance.

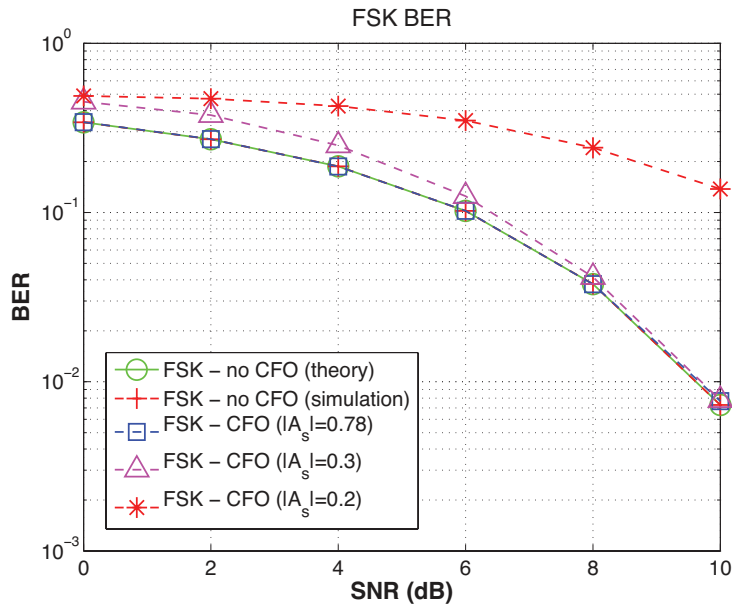


Figure 4.4: Bit error probability as a function of SNR for scatter radio FSK, for no CFO and compensated CFO scenarios with  $a_{CR} = 0$ .

### 4.1.3 Modulation Comparison

The two modulation schemes are compared in terms of BER performance in Fig. 4.5. The carrier emitter power (in dBm) is used as reference, since the SNR definitions differ for OOK and FSK, according to Eq. (3.39) and Eq. (3.63). The noise variance is the same for both modulation schemes. For OOK, the approximate-ML detector is used, and for FSK the periodogram-based CFO compensation technique is chosen. The tag's reflection coeffi-

cients are  $\Gamma_0 = 1, \Gamma_1 = -1$  and the structural term is  $A_s = 0.6047 + j0.5042$  (realistic antenna value from [21, 26]). The figure depicts the *average* BER for each modulation after 500,000 experiments. For each experiment, random channel and carrier phases are generated, and CFO is considered steady for only a small number of consecutive bits ( $N = 50$ ). Three different scenarios are presented, for three values of the emitter-to-reader channel factor:  $a_{\text{CR}} = 0.4, a_{\text{CR}} = 0.01, \text{ and } a_{\text{CR}} = 0$ .

Interestingly, it is observed that for OOK, as the channel factor drops (i.e. more attenuation), the BER drops faster. This is due to the BER averaging; recall from Eq. (3.39) that the SNR for OOK depends on the quantities  $a$  and  $b$  which are the magnitude values of the noiseless component of Eq. (3.33). These values vary randomly among the experiments due to the random channel phases they incorporate, and thus the SNR varies also. There are phase combinations that will cause the SNR of Eq. (3.39) to drop, which leads to (average) BER degradation.

That is not the case for FSK. Notice that for the latter, the BER performance is the same for any channel factor  $a_{\text{CR}}$ . Thus, FSK is a more robust communication scheme for the backscatter link, as it is immune to the channel conditions changes. Moreover, FSK fits perfectly to the concept of backscatter sensor networks, since it accounts for multiple access via frequency division multiplexing (FDM). Each sensor occupies specific, predefined subcarriers and does not collide with other sensors. Thanks to the low bitrate, the bandwidth for each sensor is very narrow, which allows many tags to be fitted in a given frequency band. FSK however, requires extra processing for CFO estimation which can be an intensive task if high FFT resolution is desired. Nevertheless, it is still preferred over OOK (which requires no intensive processing for CFO compensation), because of the “stable” BER performance at different channel conditions.

## 4.2 Achieved Bistatic Ranges

Range measurements were conducted outdoors with the setup described in Chapter 2. The RF tag (Fig. 4.6-left) was set to modulate data using the FSK

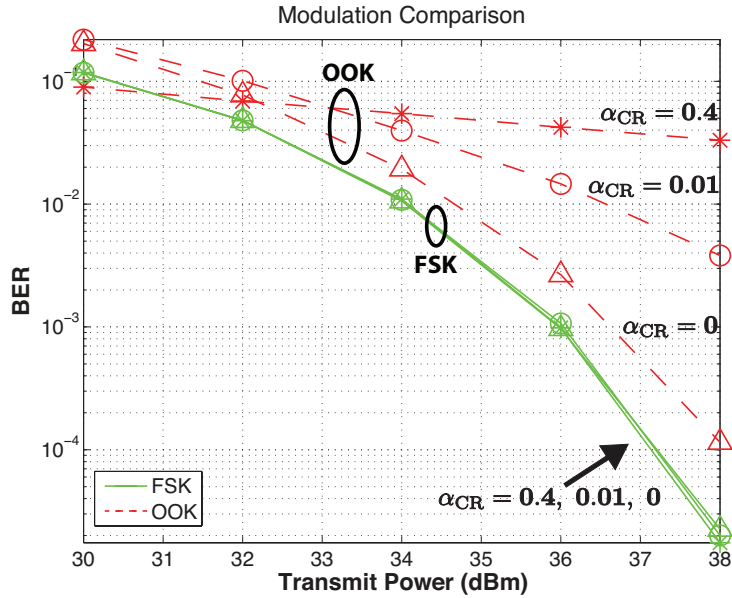


Figure 4.5: Modulation comparison for the bistatic scatter radio link. FSK and OOK compared in terms of BER as a function of the emitter transmit power and the emitter-to-reader channel factor  $\alpha_{CR}$ .

modulation scheme, at 1kbps bitrate. The carrier emitter that illuminated the tag (Fig. 4.6-right) was tuned at 867MHz, with +13dBm transmit power (20 milliwatts). The whole reception and signal processing was done with the *commodity* USRP software defined radio and a PC running custom receiver scripts. The maximum BER value measured was 5%, which for the low-bitrate scenario examined corresponds to exactly 1 erroneous bit in a packet of  $N = 20$  bits. It is noted that all the antennas were omnidirectional on the emitter, tag, and reader (monopoles). The experimental setup is shown in Fig. 4.7 and in Fig. 4.8 in a long-range deployment. Four different setups are presented, with their corresponding measurements.

#### 4.2.1 Tag close to carrier emitter

First, a tag is placed at the vicinity of the carrier emitter for different given emitter-to-reader distances (Fig. 4.9, Table 4.2.1).



Figure 4.6: Left: RF tag prototype. Right: Carrier emitter.

Table 4.1: Achieved ranges for Setup 1.

Emitter to SDR dist. $d_{CR}$	Emitter to Tag dist. $d_{CT}$	BER
> 134 m	2 m	0%
	4 m	5%
118 m	4 m	0%
	6 m	5%
84 m	8 m	0%
	9 m	3.5%
	10 m	5%
48 m	15 m	0%
	16 m	1%

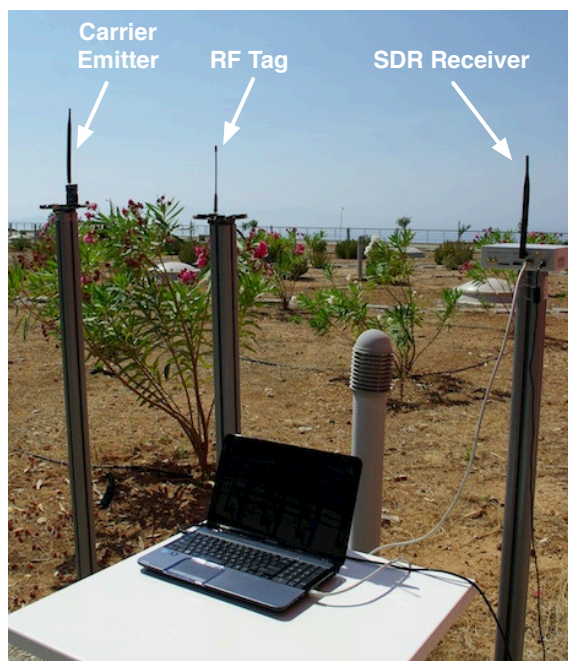


Figure 4.7: Experimental bistatic setup.



Figure 4.8: Experimental setup outdoor deployment.

### 4.2.2 Tag behind carrier emitter

Next, the tag is again placed at the vicinity of the carrier emitter, in a way that the tag-to-reader distance is longer than the emitter-to-reader distance

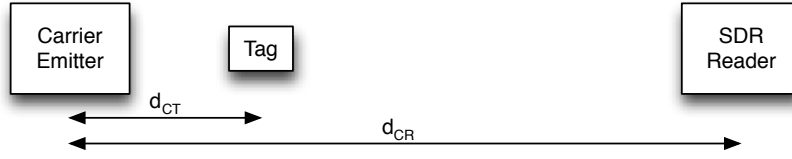


Figure 4.9: Setup 1.

(Fig. 4.10, Table 4.2.2).



Figure 4.10: Setup 2.

Table 4.2: Achieved ranges for Setup 2.

Emitter to SDR dist. $d_{CR}$	Emitter to Tag dist. $d_{CT}$	BER
48 m	12 m	0%
	14 m	5%

### 4.2.3 Tag close to reader

Then, the tag is placed at the vicinity of the reader (Fig. 4.11, Table 4.2.3).

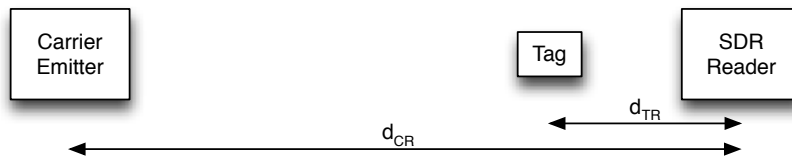


Figure 4.11: Setup 3.

### 4.2.4 Triangle topology

Finally, the setup was placed in a triangle topology, so as to fully characterize the effective range performance on a field (Fig. 4.12, Table 4.3).

Table 4.3: Achieved ranges for Setup 3.

Emitter to SDR dist. $d_{CR}$	SDR to Tag dist. $d_{TR}$	BER
48 m	17 m	0%
	24 m	2%

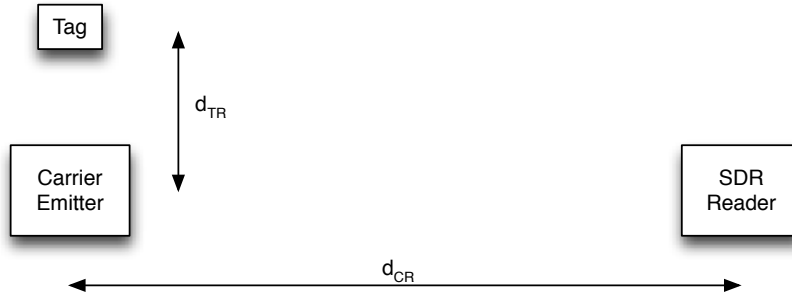


Figure 4.12: Setup 4.

Table 4.4: Achieved ranges for Setup 4.

Emitter to SDR dist. $d_{CR}$	SDR to Tag dist. $d_{TR}$	BER
100 m	3.5 m	0%
	5.5 m	5%
84 m	7.5 m	1%
	10 m	5%
48 m	15.5 m	3%
	16.5 m	5%

### 4.2.5 Results

The results are more than encouraging. For an emitter-to-reader distance of more than 134 meters, a tag may be successfully decoded up to 4 meters away from the emitter. In the measurement tables, it can be seen that as the emitter-to-reader distance decreases, the tags can be decoded successfully at much longer distances. As an example, for an emitter-to-reader distance of 48 meters, tags may be decoded successfully at 16 meters away from the emitter. In the second table, it can be seen that the tag may reach up to

14 meters *behind* the emitter for the same emitter-to-reader distance. The aforementioned essentially mean that tags are successfully decoded in an elliptical-like cell around the carrier emitter. For the same topology, when the tag is closer to the reader, ranges of up to 24 meters have been reported (third table). Finally, in a triangle topology, with an emitter-to-reader distance of 100 meters, an emitter-to-tag distance of 5.5 meters can be achieved. When the emitter-to-reader distance is reduced to 48 meters, the emitter-to-tag distance may reach up to 16 meters.

The measurements show that large-area cells may be formed at relatively long distances from the reader, and these cells' 'diameter' grows as the emitters approach the reader. The aforementioned justify the concept of cellular scatter radio architectures, where multiple carrier emitters may be placed on a field to form carrier-illuminated cells where tags reside. By strategically placing the carrier emitters, a large field coverage can be achieved, with only one reader.

### 4.3 Antenna measurements

With the setup of Fig. 4.12, a BER value of 3dB was reported with  $d_{CR} = 48\text{m}$  and  $d_{TR} = 15.5\text{m}$ . The measurements were conducted with a commercial monopole antenna for the UHF band (Fig. 4.13). For the same topology, same distances, same equipment, and different antenna, a new BER value of 1.5% was reported. A custom bow-tie antenna, designed and built in-house, was used (Fig. 4.14). The bow-tie antenna and the monopole are of equal gain in terms of dBi.

It is known that to minimize BER at the reader for binary tag modulation, the following condition is required to be met [21]:

$$\max\{|\Gamma_0 - \Gamma_1|\}. \quad (4.21)$$

Note that the definition of the load-dependent reflection coefficient of the

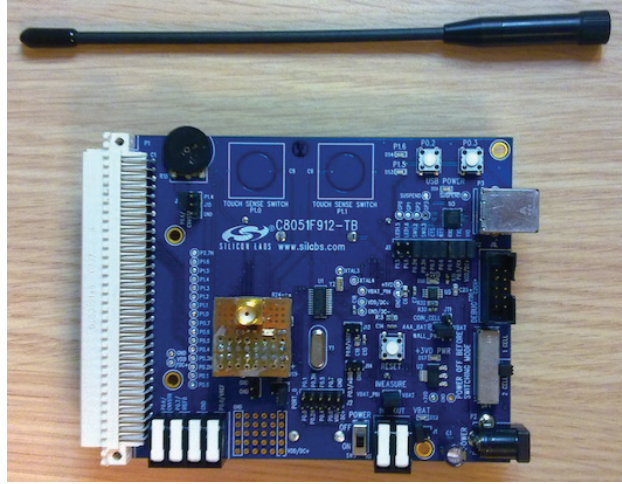


Figure 4.13: RF tag prototype with commercial monopole antenna.

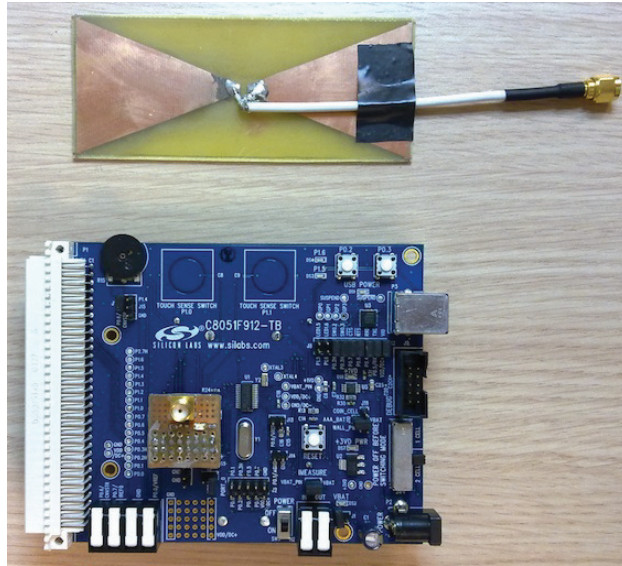


Figure 4.14: RF tag prototype with custom bow-tie antenna.

antenna-load system is

$$\Gamma_i = \frac{Z_i - Z_a^*}{Z_i + Z_a}, \quad (4.22)$$

where  $Z_i$  is the impedance value of the load  $i$ ,  $i = 0, 1$ , and  $Z_a$  is the impedance of the tag antenna at a nominal frequency. It is easily noticed

---

that  $|\Gamma_0 - \Gamma_1|$  of the condition (4.21) is a function of  $Z_a$ . Thus, BER is also a function of  $Z_a$  and this justifies that by changing the antenna, the BER is reduced.

Although a common belief in the scatter radio/RFID field is that communication performance relies on antenna load values only, it is here shown that a different antenna (with an equal gain) may lead to better BER results. Such an experimental result shows that load selection only is not sufficient for RF tag design. Load selection should accompany antenna design, to optimize tag-to-reader communication.

# Chapter 5

## Conclusions

### 5.1 Conclusion

This work aimed at low-cost environmental sensing with scatter radio technology, mainly for agricultural applications. Ultra-low cost, low power and high network density were the highest design priorities (and constraints). The bistatic scatter radio system was presented, which can be utilized to build large scale low-cost and low-power sensor networks with extended field coverage. The individual modules of the system were presented: carrier emitter and tag prototypes, along with a software-defined reader. The complete signal model was derived for the bistatic link, taking into account important tag microwave parameters. Two tag modulation schemes for information transmission were presented (OOK and FSK) and receivers were derived for both. The proposed receivers were characterized in terms of BER performance and the two modulation schemes were compared under different channel conditions. It was shown that a tag and its corresponding receiver are tied together and should be cross-designed to ensure performance maximization, which is overlooked in the backscatter/RFID field. All parameters should be taken into account while designing RF tags, combining knowledge from the microwave field (antenna load selection, antenna structural mode) and the communication field (tag modulation scheme, receiver processing). Experimentation for the proposed system was conducted with commodity SDR, to test range performance of the bistatic architecture. Impressive ranges of more than 130 meters were achieved, that show the high potential of scatter radio sensor networks built with bistatic architectures.

---

## 5.2 Future Work

This work presented the first efforts to exploit the bistatic scatter radio link for low-power and low-cost sensor digital communication. Future work should aim to further develop the aspects presented here so that full control will be taken over the bistatic link.

To totally overcome the CFO problem between the carrier emitter and the reader, a carrier tracking loop should be developed that will account for instant frequency offset fluctuations. The latter are a limiting factor when long tag transmissions are desired (i.e. bitrate reduction or number of bits per packet increase) and necessitate that a tag-transmitted packet shall not be arbitrarily large, since the CFO compensation technique described in Section 3.2.3 will perform well only during a time window where the CFO is considered steady.

The proposed receivers should be further developed to take into account the effects of the wireless channel (attenuation, channel phase), i.e. coherent receivers should be designed. This will then allow for more sophisticated communication by incorporating coding schemes to vastly reduce the BER performance. This, in turn, will result in higher achievable ranges for the scatter radio link.

New tags should be designed that account for the performance results of the proposed receivers. For example, appropriate structural mode term values should be exploited to build tags that will maximize the backscattered power per bit. In that way, the backscattered DC power may enhance the receiver's detection performance (Chapter 4). Moreover, new RF front-ends should be incorporated, e.g. MOSFET RF transistors that dissipate significantly less power than the BJT ones used throughout this work. The above should be tied with the fact that the antenna impedance value should be a crucial parameter for antenna load selection.

All the above should be combined to build large-scale scatter radio sensor networks. Questions on how to spread multiple carrier emitters on a field to illuminate hundreds of sensor tags arise: will the emitters perform FDMA or TDMA schemes? Will they be placed stochastically or with a fixed topology?

These have to be carefully investigated.

Hopefully, the expansion of this work will enable ultra low-cost and large-scale environmental sensing, which was previously unfeasible with existing technologies, both due to limiting cost and relatively high energy demands.

# Chapter 6

## Appendix

### 6.1 Proofs

#### 6.1.1 Noise PSD

At the I/Q receiver's input a Gaussian noise component  $w(t)$  is added, with power spectral density (PSD)  $N_0/2$ , around the center frequency  $F_c$ :

$$S_w(F) = \begin{cases} \frac{N_0}{2}, & |F \pm F_c| \leq W, \\ 0, & \text{elsewhere,} \end{cases} \quad (6.1)$$

where  $W$  is the receiver bandwidth. It is noted that  $w(t)$  is a narrowband wide-sense stationary (WSS) process with mean value  $\mathbb{E}[w(t)] = 0$  and autocorrelation function  $R_w(\tau) = \mathbb{E}[w(t + \tau)w(t)] = \mathcal{F}^{-1}\{S_w(F)\}$ , where  $\mathcal{F}^{-1}$  denotes the inverse Fourier transform operation. The I-branch of the demodulator mixes the incoming noise with  $\cos(2\pi F_c t)$ , resulting in

$$w'_I(t) = w(t) \cos(2\pi F_c t). \quad (6.2)$$

Then  $w'_I(t)$  is a cyclostationary process with PSD [25]:

$$S_{w'_I}(F) = \frac{1}{4}[S_w(F - F_c) + S_w(F + F_c)] = \begin{cases} \frac{N_0}{4}, & |F| \leq W, \\ \frac{N_0}{8}, & |F \pm 2F_c| \leq W, \\ 0, & \text{elsewhere.} \end{cases} \quad (6.3)$$

After low-pass filtering (elimination of frequencies above  $\pm W$ ), a noise component  $n_I(t)$  is obtained, with PSD

$$S_{n_I}(F) = \begin{cases} \frac{N_0}{4}, & |F| \leq W, \\ 0, & \text{elsewhere.} \end{cases} \quad (6.4)$$

The same apply for the Q-branch of the demodulator, which yields the noise component  $n_Q(t)$ .

### 6.1.2 Orthogonality of FSK base functions

For correlation-demodulation of noncoherent FSK, signal orthogonality has to be guaranteed between the basis functions of each frequency. Two basis functions are orthogonal iff

$$\int_0^T (e^{j2\pi F_i t}) (e^{j2\pi F_j t})^* dt = 0, \quad (6.5)$$

for any two frequencies  $F_i, F_j$ , or equivalently,

$$\int_0^T e^{j2\pi(F_i - F_j)t} dt = 0. \quad (6.6)$$

Beginning with an arbitrary frequency  $F_0$ , a second frequency  $F_1$  is chosen, so that Eq. (6.6) holds. The necessary condition for this is  $|F_0 - F_1| = k\frac{1}{T}$ ,  $k \in \mathbb{N}$ .

Orthogonality of frequencies  $F_i$  and  $-F_i$ , is also guaranteed, for every  $i$ . This is because

$$\int_0^T (e^{j2\pi F_i t}) (e^{j2\pi(-F_i)t})^* dt = \int_0^T e^{j2\pi 2F_i t} dt, \quad (6.7)$$

where the last integral's value may be considered zero for  $2F_i \gg 1/T$ , which is true for low bitrate scenarios. Similarly, for any pair  $\{F_0, -F_1\}, \{-F_0, F_1\}$

it can be seen that

$$\int_0^T (e^{j2\pi F_0 t}) (e^{j2\pi(-F_1)t})^* dt = \int_0^T e^{j2\pi(F_0+F_1)t} dt, \quad (6.8)$$

where the integral's value may be considered zero for  $F_0 + F_1 \gg 1/T$ .

### 6.1.3 Noise Variance for FSK receiver BER

At the FSK correlator's outputs, the statistics are of the form

$$r_i^+ = \psi + \sum_{k=0}^{L-1} n[k], \quad (6.9)$$

where  $\psi$  is a constant, and  $n[k] \sim \mathcal{CN}(0, 2\sigma_n^2)$ . Because  $n[k]$  are i.i.d. complex Gaussian variables for any  $k$ , the sum is a complex Gaussian variable with variance equal to the sum of the variances of  $L$  independent  $n[k]$  variables, i.e.  $2L\sigma_n^2$ . Then  $r_i^+ \sim \mathcal{CN}(\psi, 2L\sigma_n^2)$ ; i.e.  $r_i^+ \triangleq r_{i,I}^+ + j r_{i,Q}^+$  follows the complex Gaussian distribution, with  $r_{i,I}^+, r_{i,Q}^+$  real and Gaussian distributed, each having a zero mean value, and variance  $L\sigma_n^2$ .

Each statistic  $z_i, i = 0, 1$  has the form

$$z_i = |r_i^+|^2 + |r_i^-|^2 = (r_{i,I}^+)^2 + (r_{i,Q}^+)^2 + (r_{i,I}^-)^2 + (r_{i,Q}^-)^2, \quad (6.10)$$

which is a sum of four squared real Gaussian rv's, each with variance  $\sigma^2 = L\sigma_n^2$ . Thus,  $z_i$  is a chi-squared rv with 4 degrees of freedom (or a non-central chi-squared rv with 4 degrees of freedom, depending on the value of  $\psi$ ).

## 6.2 RF Tag Schematics & Bill of Materials

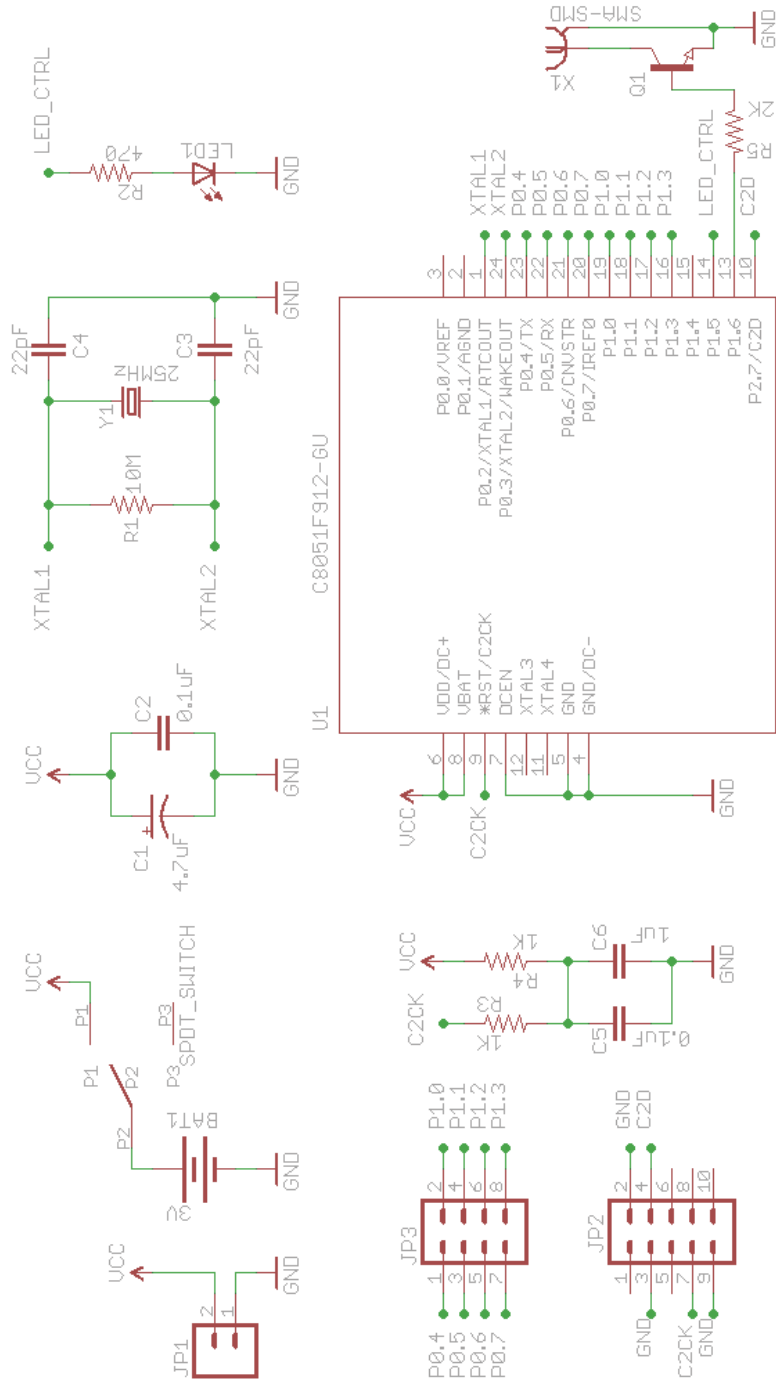


Figure 6.1: RF tag schematic.



Table 6.1: Bill of Materials for semipassive RF tag.

<b>Part</b>	<b>Value</b>	<b>Package</b>
C1	4.7uF TANT	1206
C2	0.1uF	0805
C3, C4	22pF	0603
C5	0.1uF	0603
C6	1uF	0603
R1	10M $\Omega$	0603
R2	470 $\Omega$	0603
R3, R4	1K $\Omega$	0603
R5	2K $\Omega$	0805
LED	Green LED	1206
Y1	25MHz Crystal Oscillator	Through-hole
U1	C8051F912-GU MCU	24QSOP
Q1	AT-32033 NPN Transistor	SOT-23
X1	SMA Connector Vertical	SMD
JP1	Power Supply Connector	2x1 DIP Header
JP2	C2 Programming Connector	5x2 DIP Header
JP3	GPIO Connector	4x2 DIP Header
BAT1	CR2032 Coin Cell Battery Holder	
SPDT	SPDT Slide switch	Through-hole

# Bibliography

- [1] W. Zhang, G. Kantor, and S. Singh, “Integrated wireless sensor/actuator networks in an agricultural application,” in *Proc. ACM Conf. on Embed. Net. Sens. Sys. (SenSys)*, Nov. 2004, p. 317, Baltimore, USA.
- [2] T. Wark, P. Corke, P. Sikka, L. Klingbeil, Y. Guo, C. Crossman, P. Valencia, D. Swain, and G. Bishop-Hurley, “Transforming agriculture through pervasive wireless sensor networks,” *IEEE Pervasive Computing*, vol. 6, no. 2, pp. 50–57, 2007.
- [3] G. Vellidis, M. Tucker, C. Perry, C. Kvien, and C. Bednarz, “A real-time wireless smart sensor array for scheduling irrigation,” *Computers and Electronics in Agriculture*, vol. 61, no. 1, pp. 44–50, 2008.
- [4] I. Akyildiz, W. Su, Y. Sankarasubramaniam, and E. Cayirci, “Wireless sensor networks: a survey,” *Computer Networks*, vol. 38, no. 4, pp. 393–422, 2002.
- [5] D. M. Dobkin, *The RF in RFID: Passive UHF RFID in Practice*. Newnes (Elsevier), 2008.
- [6] H. Stockman, “Communication by means of reflected power,” *Proc. IRE*, pp. 1196–1204, 1948.
- [7] *EPC Radio-Frequency Identity Protocols, Class-1 Generation-2 UHF RFID Protocol for Communications at 860 MHz-960 MHz, version 1.2.0*. EPC Global, 2008.
- [8] A. Sample, D. Yeager, P. Powledge, and J. Smith, “Design of a passively-powered, programmable sensing platform for uhf rfid systems,” in *IEEE Intl. Conf on RFID 2007*, Grapevine, TX, Mar. 2007, pp. 149–156.

- 
- [9] G. Vannucci, A. Bletsas, and D. Leigh, "A software-defined radio system for backscatter sensor networks," *IEEE Trans. Wireless Commun.*, vol. 7, no. 6, pp. 2170–2179, Jun. 2008.
- [10] V. Lakafosis, A. Rida, R. Vyas, L. Yang, S. Nikolaou, and M. M. Tentzeris, "Progress towards the first wireless sensor networks consisting of inkjet-printed, paper-based rfid-enabled sensor tags," *Proc. IEEE*, vol. 98, no. 9, pp. 1601–1609, Sep. 2010.
- [11] J. Kimionis, A. Bletsas, and J. N. Sahalos, "Design and implementation of RFID systems with software defined radio," in *6th IEEE European Conference on Antennas and Propagation (EUCAP)*, Prague, Czech Republic, Mar. 2012, pp. 3464–3468.
- [12] J. D. Griffin and G. D. Durgin, "Complete link budgets for backscatter-radio and rfid systems," *IEEE Antennas Propagat. Mag.*, vol. 51, no. 2, pp. 11–25, Apr. 2009.
- [13] D. Tse and P. Viswanath, *Fundamentals of Wireless Communication*. Cambridge University Press, 2005.
- [14] D. Kim, M. A. Ingram, and J. W. Whit Smith, "Measurements of small-scale fading and path loss for long range RF tags," *IEEE Trans. Antennas Propagat.*, vol. 51, no. 8, pp. 1740–1749, Aug. 2003.
- [15] A. Sample, J. Braun, A. Parks, and J. Smith, "Photovoltaic enhanced UHF RFID tag antennas for dual purpose energy harvesting," in *IEEE Intl. Conf on RFID*, Orlando, FL, Apr. 2011, pp. 146–153.
- [16] D. D. Donno, F. Ricciato, L. Catarinucci, A. Coluccia, and L. Tarricone, "Challenge: Towards distributed RFID sensing with software-defined radio," in *16th Annual Intl. Conf on Mobile Computing and Networking (ACM MobiCom)*, Chicago, IL, 2010, pp. 97–104.
- [17] M. Buettner and D. Wetherall, "A 'Gen 2' RFID monitor based on the USRP," *ACM SIGCOMM Computer Communication Review*, vol. 40, no. 3, pp. 42–47, Jul. 2010.

- 
- [18] J. Kimionis, “Design and implementation of backscatter links with software defined radio for wireless sensor network applications,” Diploma Thesis, Technical University of Crete, 2011, supervisor A. Bletsas.
- [19] S. Thomas, E. Wheeler, J. Teizer, and M. Reynolds, “Quadrature amplitude modulated backscatter in passive and semipassive UHF RFID systems,” *IEEE Trans. Microwave Theory Tech.*, vol. 60, no. 4, pp. 1175–1182, Apr. 2012.
- [20] C. A. Balanis, *Antenna Theory: Analysis and Design*, 3rd ed. New Jersey: John Wiley and Sons, 2005.
- [21] A. Bletsas, A. G. Dimitriou, and J. N. Sahalos, “Improving backscatter radio tag efficiency,” *IEEE Trans. Microwave Theory Tech.*, vol. 58, no. 6, pp. 1502–1509, Jun. 2010.
- [22] M. K. Simon, *Probability Distributions Involving Gaussian Random Variables: A Handbook for Engineers and Scientists*. New York, NY, 10013: Springer Science and Business Media LLC, 2002.
- [23] J. G. Proakis, *Digital Communications*, 4th ed. New York, NY, 10020: McGraw-Hill, Inc., 2001.
- [24] M. Abramowitz and I. A. Stegun, *Handbook of Mathematical Functions with Formulas, Graphs, and Mathematical Tables*. Washington, D.C.: United States Department of Commerce, 1970.
- [25] J. G. Proakis and M. Salehi, *Communication Systems Engineering*, 2nd ed. Prentice-Hall, 2002.
- [26] C.-C. Yen, A. E. Gutierrez, D. Veeramani, and D. van der Weide, “Radar cross-section analysis of backscattering RFID tags,” *IEEE Antennas and Wireless Propagation Letters*, vol. 6, pp. 279–281, 2007.